GNAO1 organizes the cytoskeletal remodeling and firing of developing neurons

赤峰, 哲

Received: 8 May 2020 | Revised: 3 September 2020 | Accepted: 13 October 2020

DOI: 10.1096/fj.202001113R

RESEARCH ARTICLE

THE FASEB JOURNAL

GNAO1 organizes the cytoskeletal remodeling and firing of developing neurons

Satoshi Akamine[1] | Sayaka Okuzono[1] | Hiroyuki Yamamoto[1] | Daiki Setoyama[2] | Noriaki Sagata[3] | Masahiro Ohgidani[3] | Takahiro A. Kato[3] | Tohru Ishitani[4,5] | Hiroki Kato[6] | Keiji Masuda[7] | Yuki Matsushita[1] | Hiroaki Ono[1] | Yoshito Ishizaki[1] | Masafumi Sanefuji[1] | Hirotomo Saitsu[8] | Naomichi Matsumoto[9] | Dongchon Kang[2] | Shigenobu Kanba[3] | Yusaku Nakabeppu[10] | Yasunari Sakai[1] | Shouichi Ohga[1]

[1]Department of Pediatrics, Graduate School of Medical Sciences, Kyushu University, Fukuoka, Japan

[2]Department of Clinical Chemistry and Laboratory Medicine, Graduate School of Medical Sciences, Kyushu University, Fukuoka, Japan

[3]Department of Neuropsychiatry, Graduate School of Medical Sciences, Kyushu University, Fukuoka, Japan

[4]Division of Integrated Signaling Systems, Institute for Molecular and Cellular Regulation, Gunma University, Maebashi, Japan

[5]Department of Homeostatic Regulation, Division of Cellular and Molecular Biology. Research Institute for Microbial Diseases, Osaka University, Suita, Japan

[6]Division of Oral Biological Sciences, Department of Molecular Cell Biology and Oral Anatomy, Graduate School of Dental Science, Kyushu University, Fukuoka, Japan

[7]Section of Oral Medicine for Children, Division of Oral Health, Growth and Development, Faculty of Dental Science, Kyushu University, Fukuoka, Japan

[8]Department of Biochemistry, Hamamatsu University School of Medicine, Hamamatsu, Japan

[9]Department of Human Genetics, Yokohama City University Graduate School of Medicine, Yokohama, Japan

[10]Division of Neurofunctional Genomics, Department of Immunobiology and Neuroscience, Medical Institute of Bioregulation, Kyushu University, Fukuoka, Japan

Correspondence
Yasunari Sakai, Department of Pediatrics, Graduate School of Medical Sciences, Kyushu University, Fukuoka 812-8582, Japan.
Email: ysakai22q13@gmail.com

Funding information
JSPS KAKENHI, Grant/Award Number: JP19K08281 and JP17H01539; AMED, Grant/Award Number: JP19ek0109411, JP19ek0109280, JP19ek0109348 and JP18kk020501; Health and Labour Sciences Research Grant; Ministry of Health, Labour and Welfare of Japan; Life Science Foundation of Japan; Takeda Science Foundation; The Mother and Child Health

Abstract

Developmental and epileptic encephalopathy (DEE) represents a group of neurodevelopmental disorders characterized by infantile-onset intractable seizures and unfavorable prognosis of psychomotor development. To date, hundreds of genes have been linked to the onset of DEE. *GNAO1* is a DEE-associated gene encoding the alpha-O1 subunit of guanine nucleotide-binding protein ($G\alpha_O$). Despite the increasing number of reported children with *GNAO1* encephalopathy, the molecular mechanisms underlying their neurodevelopmental phenotypes remain elusive. We herein present that co-immunoprecipitation and mass spectrometry analyses identified another DEE-associated protein, SPTAN1, as an interacting partner of $G\alpha_O$. Silencing of endogenous *Gnao1* attenuated the neurite outgrowth and calcium-dependent signaling. Inactivation of *GNAO1* in human-induced pluripotent stem cells gave rise to

Abbreviations: AIS, axonal initial segment; Ankyrin-G, AnkG; DEE, developmental and epileptic encephalopathy; *GNAO1*, *G protein subunit alpha O1*; $G\alpha_O$, alpha-O1 subunit of guanine nucleotide-binding protein (the protein encoded by *GNAO1*); iPSCs, induced pluripotent stem cells; MO, morpholino antisense oligonucleotides; SHEDs, stem cells from human exfoliated deciduous teeth; SPTAN1, spectrin alpha, non-erythrocytic 1; TUBB3, tubulin beta III.

Foundation; The Japan Epilepsy Research Foundation; Kawano Masanori Memorial Public Interest Incorporated Foundation for Promotion of Pediatrics

anomalous brain organoids that only weakly expressed SPTAN1 and Ankyrin-G. Furthermore, *GNAO1*-deficient organoids failed to conduct synchronized firing to adjacent neurons. These data indicate that $G\alpha_O$ and other DEE-associated proteins organize the cytoskeletal remodeling and functional polarity of neurons in the developing brain.

KEYWORDS

cytoskeleton, developmental and epileptic encephalopathy, *G protein subunit alpha O1 (GNAO1)*, organoid, spectrin alpha, non-erythrocytic 1 (SPTAN1)

1 | INTRODUCTION

Epileptic encephalopathy represents a heterogeneous group of epileptic syndromes in childhood characterized by intractable seizures and developmental delay.[1,2] Among the various forms of epileptic encephalopathy, children with infantile-onset seizures are known to follow the most severe course in the seizure control and developmental outcome. This group of patients is therefore defined as having "developmental epileptic encephalopathy (DEE)".[3] Based on the time of onset and types of seizure, DEE is further classified into early-infantile epileptic encephalopathy (also known as Ohtahara syndrome),[4] early myoclonic encephalopathy,[5] migrating partial seizures in infancy,[6] and other subgroups.[3] Recent studies have suggested that epilepsy and developmental outcomes are two related neurological phenotypes resulting from various genetic backgrounds.[7]

Exome sequencing provides evidence that individuals with DEE carry rare de novo variations in genes that organize neuronal differentiation and synaptogenesis.[7] To date, hundreds of genes have been identified to be associated with DEE.[2,8] Among them, *GNAO1* is one of recently identified genes,[9] and the number of reported cases with DEE due to de novo *GNAO1* mutations is increasing.[10-14] Patients with *GNAO1* mutations show a variety of epileptic and non-epileptic phenotypes, including severe developmental delay, hypotonia, and involuntary movements.[15] Affected children thus received the diagnosis of early infantile epileptic encephalopathy-17 (OMIM #615473), neurodevelopmental disorder with involuntary movements (OMIM #617493), or alternatively designated as an autosomal dominant disorder, "*GNAO1*-associated encephalopathy".[11]

GNAO1 encodes an alpha subunit of heterotrimeric GTP-binding protein (designated hereafter as $G\alpha_O$), one of the most abundant proteins in mammalian brains.[16] The GTP-bound form of $G\alpha_O$ activates its functionally associated molecules, such as phospholipase C and calcium channels. Thus, activated signals downstream from $G\alpha_O$ regulate neuronal excitability and firing.[17,18] Postnatal mice lacking $G\alpha_O$ show epileptiform discharges, spontaneous seizures, and motor impairments from an early age.[19,20] These data clearly indicate that $G\alpha_O$ performs essential functions in the postnatal brain; however, whether $G\alpha_O$ organizes molecular pathways cooperatively with other DEE-associated proteins in the developing brain is unclear.

In the present study, we report that $G\alpha_O$ physically interacts with spectrin alpha 1 (SPTAN1), another DEE-associated protein.[21-23] Using the neuronal differentiation system in vitro from induced pluripotent stem cells (iPSCs), we demonstrate that *GNAO1* performs a novel function in cytoskeletal remodeling in neurons. Our experimental data indicate that the functional loss of *GNAO1* impairs neural polarity and connectivity in the developing brain.

2 | MATERIALS AND METHODS

2.1 | Ethics statement

All experimental methods were carried out in stringent compliance with the institutional guidelines and protocols approved by the Institutional Review Board at Kyushu University (23-53, 28-88, 29-393, and 678-01). Informed consent was obtained from the healthy donors of blood cells, the parents of patients, and the parents of donor children for mesenchymal stem cells in deciduous teeth, prior to the acquisition of human samples. For animal experiments, specific protocols were approved by the Institutional Animal Care and Use Committee (A29-254-1).

2.2 | Animals

Wild-type (WT) C57BL/6 J mice were maintained in a specific-pathogen-free environment. The animals had ad libitum access to food and water at all times, and the temperature was maintained at 25°C with a 12-hour light-dark cycle.

2.3 | Quantitative real-time PCR

Total RNA was extracted with an RNeasy Mini Kit (Qiagen Inc, Germantown, MD, USA) for samples.[24] Complementary DNA was synthesized using a

High-Capacity RNA to cDNA Kit (Life Technologies, Carlsbad, CA, USA) according to the manufacturer's protocol. Assays were carried out using the SYBR Green system (Thermo Fisher Scientific, Waltham, MA, USA). The delta-delta cycle threshold algorithm was applied for the quantitative measurement of the mRNA expression. Human or murine homolog of actin beta (ACTB) was used as an internal control. Sequences of oligonucleotide primers are provided in Extended data (Table S1).

2.4 | Immunofluorescence study

Cultured cells were fixed with 4% paraformaldehyde (PFA) in phosphate-buffered saline (PBS, pH 7.4) for 15 minutes and permeabilized with 0.1% Triton X-100 for 10 minutes.[25] Animals were deeply anesthetized and perfused with 4% PFA in ice-cold PBS. The brain was dissected and immediately immersed in 4% PFA overnight. The fixed brain was then cryo-protected with 20% and 30% sucrose-containing PBS at 4°C for 24 hours each and then frozen in optimal cutting temperature (OCT) compound (Sakura Finetek, Tokyo, Japan). Fixed samples were serially cut into 40-μm-thick slices. Samples were then blocked with Block Ace (KAC Co. Ltd., Kyoto, Japan) and incubated overnight at 4°C with primary antibodies. Alexa 488, 555, and 647 (Life Technologies) were used as the secondary antibodies. The fluorescence dye of 4′,6-diamidino-2-phenylindole (DAPI) was used for nuclear staining. The signal intensity of an immunolabeled protein in the region of interest (ROI) was measured for a quantitative analysis using the NIS-elements AR software program (Nikon Corporation, Tokyo, Japan).

2.5 | Co-immunoprecipitation

Neuro2a cells stably expressing GFP or $G\alpha_O$-GFP fusion proteins (Figure S1) were grown on 10-cm dishes. Logarithmically proliferating, 1-2 × 10^8 cells were collected on ice with lysis buffer (150 mM NaCl, 2 mM EDTA, 20 mM Tris-HCl [pH 7.5], and 1% Triton X-100) supplemented with protease inhibitor cocktail (Roche Diagnostics, Rotkreuz, Switzerland). Whole-cell lysates were adjusted to 15-20 mg/mL total protein, and the total volume was set to 1 mL with 1% bovine hemoglobin (Sigma-Aldrich, St. Louis, MO, USA)-containing lysis buffer. Pre-cleaning of the lysates was carried out with 1% hemoglobin-coated protein A- or protein G-agarose beads on a rotating machine for 1 hour at 4°C. After recovering the supernatants of precleaned lysates, GFP or $G\alpha_O$-GFP protein complex was immunoprecipitated with 50 μL slurry of anti-GFP monoclonal antibody (JL-8) magnetic beads (MBL Co. Ltd., Nagoya, Japan) at 4°C overnight. Whole amounts of bead-captured proteins were extracted with 20 μL Laemmli sampling buffer containing 2-mercaptoethanol (1%). Boiled samples were subjected to sodium dodecyl sulfate-polyacrylamide gel electrophoresis (SDS-PAGE; 4%-15% Mini-PROTEAN TGX Gels; BioRad Laboratories, Hercules, CA, USA). Protein bands were detected with Coomassie Brilliant Blue (CBB) staining. Extracts from the wild-type mouse brain were used for Co-IP as previously described.[26] Briefly, cortical hemispheres were dissected from 6-week-old male mice. The homogenates were freshly prepared from dissected brains in the same lysis buffer as described above. Supernatants after the 14 000-rpm centrifugation twice were defined as the brain extract. Brain extracts containing 4 mg of total protein were adjusted to 500 μL with lysis buffer, and subjected to the immunoprecipitation with 5 μg mouse anti-SPTAN1 antibody (Clone D8B7, Abcam ab11755) or the pre-immune isotype of mouse IgG2b (ab18469). After immunoprecipitation (rotor incubation at 4°C for 2 hours) and extensive washing for four times, eluted proteins were analyzed with western blotting.

2.6 | Western blotting

The standard protocol was followed, as previously described.[25] After SDS-PAGE, separated proteins were transferred to a PVDF membrane (Trans-Blot Turbo Transfer Pack; BioRad). The blotted membranes were incubated at 4°C overnight in 5% milk, PBS-T buffer (0.1% Triton-X and PBS, pH 7.4) and primary antibodies. Horseradish peroxidase (HRP)-linked anti-mouse or anti-rabbit light-chain-specific secondary antibodies (211-032-171, 115-035-174; Jackson ImmunoResearch, West Grove, PA, USA) were used to detect chemiluminescence signals (Clarity ECL substrate, BioRad; and ImmunoStar LD, FUJIFILM Wako Pure Chemical Corporation, Osaka, Japan). Image acquisitions and quantitative analyses were performed using the FluorChem FC2 System software program (ProteinSimple, San Jose, CA, USA). ACTB was used as an internal control. Information on antibodies is summarized in Extended data.

2.7 | Liquid chromatography with tandem mass spectrometry

After CBB staining, the protein band-positive regions of gels were cut into 1-mm squares and subjected to in-gel digestion, as previously described.[27] Trypsin-digested peptide was separated using the Easy-nLC 1000 system (Thermo Fisher Scientific) with an Acclaim PepMap 100 trap column (20 × 0.075 mm; 3 μm) and Acclaim PepMap RSCL analytical column (150 × 0.05 mm; 2 μm) and analyzed using a Q-Exactive Orbitrap mass analyzer (ThermoScientific). Data were analyzed using the Proteome Discoverer software program

(ThermoScientific) for protein identification with the Sequest HT algorithm against the human protein Uniprot database.[28]

2.8 | Microscopic analyses

Confocal images were obtained with A1 HD25 (Nikon), as previously described.[25] The all-in-one microscope BZ-X800 equipped with the analytical software program BZ-X analyzer (Keyence, Osaka, USA) was used for the quantitative analysis of morphological features. To acquire deep images, 4% PFA-fixed organoids were treated with ScaleView-A2 reagents (Fujifilm-Wako, Osaka, Japan). BZ-X800 and Spin SR10 microscopes (Olympus, Tokyo, Japan) were used for deep imaging (615-705 μm in-depth).

2.9 | Direct conversion of human fibroblasts to neurons

An established method was used for the in vitro differentiation of neurons from human fibroblasts.[29] Commercially available fibroblasts from healthy volunteers were purchased from Coriell Institute for Medical Research (Camden, NJ, USA). The direct reprogramming system with three transcription factors (ASCL1, MYT1L, and POU3F2) was used to convert cultured fibroblasts to neurons in vitro. Fresh medium was replaced every 3 days with appropriate antibiotics to select infected cells. Induced neuronal cells were collected at 14 days after infection.

2.10 | In vitro differentiation of neurons from mesenchymal stem cells

Stem cells from human exfoliated deciduous teeth (SHEDs) were obtained to induce dopaminergic neurons in vitro, as described.[30] SHEDs (1×10^5 cells) were transferred to a 6-well culture plate, and dopaminergic neurons were induced for 5 days in the culture media containing neurobasal medium (Life Technologies) supplemented with 2% B27 supplement (Life Technologies), 1 mM dibutyryladenosine 3,5-cyclic monophosphate (Sigma-Aldrich), 0.5 mM 3-isobutyl-1-methylxanthine (Sigma-Aldrich), 200 μM ascorbic acid (Nacalai Tesque, Kyoto, Japan), and 50 ng/mL BDNF. Total RNA was recovered from these neurons at 10 days of DIV and subjected to quantitative PCR analyses.

2.11 | Establishment of induced pluripotent stem cells (iPSCs)

Peripheral blood mononuclear cells (PBMNCs) were activated with Dynabeads human T-Activator CD3/CD28 (Thermo Fisher Scientific) in KBM502 medium (Kohjin Bio Co., Saitama, Japan) for 6 days. Activated T-cells (2.5×10^5 cells) were suspended in 350 μL of KBM502 medium with CytoTune-iPS 2.0 (DNAVEC, Tokyo, Japan) at a multiplicity of infection (MOI) of 6 and cultivated in a 24-well plate for the next 72 hours Control cells from a healthy volunteer (lab ID: 956P) were plated on a 6-well plate coated with the recombinant laminin-511 E8 fragments (iMatrix-511; Nippi Inc, Tokyo, Japan) in StemFit AK03 (Ajinomoto, Tokyo, Japan). Approximately 20-30 days after infection, colonies of iPSCs were selected. The same protocol was applied for the establishment of iPSCs from patients with GNAO1 encephalopathy. The iPSCs were expanded on mitomycin C-inactivated SNL feeder cells in Primate ES medium containing bFGF.

All iPSCs expressed the stem cell-specific markers TRA-1-60, NANOG, SSEA4, OCT4, and ALP on immunofluorescence or immunohistochemistry (ES/iPS Cell, Human, Characterization Kit; SAB-KIT-1; System Biosciences, Palo Alto, CA, USA). At 21 days after embryoid body formation, an immunofluorescence analysis also confirmed the differentiation of iPSCs into three embryonic germ layers based on the markers of AFP (endoderm), SMA (mesoderm), and TUJI (ectoderm) (3-Germ Layer Immunocytochemistry Kit; ThermoFisher Scientific). All iPSC clones were completely clear of Sendai virus DNA by passage 16 (iPS Transgene/SeV detection primer kit; IDT-DV0301; MBL). G-banded karyotyping excluded chromosomal abnormalities in iPSCs on passage 10 (Chromocenter Inc, Yonago, Japan). Established iPSCs were cultured on Matrigel (Corning Inc, Corning, NY, USA) in mTeSR1 medium (STEMCELL Technologies Inc, Vancouver, Canada). The medium was changed every day, and cells were passaged every 5 days using TrypLE Select (ThermoFisher Scientific) and Rho-kinase inhibitor Y27632 (Wako).

2.12 | CRISPR/Cas9 system

The target sequences for CRISPR were designed at CRISPR direct (http://crispr.dbcls.jp/).[31] The insert oligonucleotides for human *GNAO1* guide RNA (gRNA) were CACCGAATCGCCTTGCTCCGCTCGA and AAACTCG AGCGGAGCAAGGCGATTC (5′ to 3′). The complementary oligonucleotides for gRNA were annealed and cloned into a pX459 CRISPR/Cas9-Puro vector (Addgene, Cambridge, MA, USA).[32] A total of 2.0×10^5 cells were electroporated at 1275 V, 10 msec, 3 pulses using 10-μL tips (Thermo Fisher Scientific) with 1 μg of pX459/GNAO1 gRNA. The cells were plated onto basement membrane matrix-coated plates in mTeSR1 medium. Forty-eight hours after electroporation, cells were cultured in selection medium containing 0.5 μg/mL puromycin for 3 days and allowed to recover for the following

3 weeks. Puromycin-resistant colonies were manually selected and expanded for genotyping. The genomic DNA was extracted with a Qiagen DNA blood mini Kit (Qiagen). PCR was performed with TaKaRa LA Taq with GC Buffer (Takara Bio Inc, Kusatsu, Japan), according to the manufacturer's instructions. The following primers were designed to amplify exon 1 of *GNAO1* (5′ to 3′): CTCCGCTGCTGGAATCTTGT and GGGACTAAGGCATGCGAGG. The PCR product was purified with a QIAquick PCR Purification Kit (Qiagen) and cloned into the EcoRV site of the pBluescript II SK- vector (Agilent Technologies, Santa Clara, CA, USA) with a Mighty Cloning Reagent Set, Blunt End (Takara Bio Inc). Sequencing of *GNAO1* was performed with the PCR primers for 8 colonies.

2.13 | Neuronal differentiation of iPSCs

Cortical neurons were differentiated from iPSCs using the serum-free floating culture of embryoid body-like aggregates with quick reaggregation (SFEBq) method.[33] In brief, iPSCs were pretreated for 3 hours with 50 μM Y27632 (FUJIFILM Wako), dissociated with TrypLE Express (ThermoFisher Scientific), and quickly reaggregated using low cell-adhesion 96-well culture plates (10 000 cells/well, 150 μL) in the following differentiation medium: DMEM/Nutrient Mixture F-12 Ham, containing Knockout Serum Replacement (ThermoFisher Scientific) and MEM nonessential amino acids solution, L-glutamine, 2-mercaptoethanol (Nacalai Tesque, Inc). The medium was replenished every four days. Rho-kinase, ALK5 tyrosine kinase, and AMP-kinase inhibitors (Y27632 [50 μM], SB431542 [10 μM, Sigma], and dorsomorphin dihydrochloride [2 μM, Tocris Bioscience, Abingdon, UK) were added to the differentiation medium from days 0 to 4. On day 18, cell aggregates were transferred to a nonadhesive dish and cultured in Neurobasal Medium supplemented with B27 and L-glutamine. For the morphological analysis of single neurons, neuro-spheroids and organoids were plated onto iMatrix 511-pretreated 35-mm cover glasses (Matsunami Glass Ind. Ltd., Kishiwada, Japan).

2.14 | Short-interfering (si)RNAs

Neuro2a cells were chemically transfected with Lipofectamine RNA iMAX (ThermoFisher Scientific) and 100 μM of siRNAs (Sigma) harboring the following sequences (5′ to 3′): siGnao1 CUGAACCGUUCUCUGCAGATT and 5′-UCUG CAGAGAACGGUUCAGTT. Stealth RNAi Negative Control Low GC Duplex(es) (CUUCAAUCCUAAGACGAGAtt and UCUCGUCUUAGGCUUGAAGta; Life Technologies) were used as controls, as previously described.[24] The knockdown effects were assessed with qPCR and Western blotting 48 to 72 hours after transfection.

2.15 | Morpholino antisense oligonucleotides

Zebrafish (Danio rerio) were raised and maintained under standard conditions. Morpholino antisense oligonucleotides (MOs) were obtained from Gene Tools (Philomath). For all injections, 5 ng of control MO, gnao1a MO, or p53 MO was micro-injected under the stereomicroscope at the single-cell stage of fertilized eggs. The following sequences of MO were designed (5′ to 3′): gnao1a CATGGCTAGATGAACCTCGGCTCTT, p53 GCGCCATTGCTTTGCAAGAATTG, and gnao1a 5-mis (control) CATcGCTAcATcAACCTCcGCTaTT. The five mismatched sequences in control MO were shown in lowercase. p53 MO was used to prevent embryos from undergoing apoptosis due to the manipulation and MO injection.[34]

2.16 | Calcium imaging

WT and GNAO1 KO organoids at 120-150 days of differentiation were plated onto iMatrix-511-coated cover slips, on which neurons spread their neurites over the next 100 days of culture. Neurons were then pretreated with Calcium Kit-Fluo4 (Dojindo Laboratories, Kumamoto, Japan) and stimulated with 100 μM ionomycin. Oscillating intracellular calcium levels were detected as the argon laser-activated Fluo4-AM signal in the 488-nm channel of an A1 confocal microscope (Nikon) using the software program NIS-Elements AR. Live-cell imaging at 0 to 10 minutes after stimulation was recorded at 300-msec intervals.

2.17 | Luciferase assay

Dual luciferase assays were performed according to the manufacturer's protocol (Promega, Madison, WI, USA). The firefly luciferase reporters containing AP-1 (3xAP-1pGL3, #40342)[35] and CTNNB1-binding sites (M50 Super 8x TOPFlash, #12456) were purchased from Addgene (Watertown, MA, USA).

2.18 | Experimental design and statistical analyses

At least three independent animals, cultured cells and organoids were prepared, and were analyzed for experiments. All of the statistical analyses were performed using the JMP software program (SAS Institute, Cary, NC, USA). The collected data are presented

as the mean ± standard deviation (SD) unless otherwise stated. Wilcoxon's rank sum test was used as a nonparametric method. P values of <.05 were considered statistically significant.

3 | RESULTS

3.1 | Physical interaction between $G\alpha_O$ and SPTAN1

To investigate the molecular functions of $G\alpha_O$, we performed co-immunoprecipitation (Co-IP) and mass spectrometry analyses with Neuro2a cells stably expressing GFP only or GFP-tagged $G\alpha_O$ fusion protein (Figure 1A and Figure S1A). Mass spectrometry identified a total of 1057 unique peptides (Table S2), and the proteomic algorithm predicted that these peptides were the ionized products of 47 different proteins. We therefore considered these proteins to be the components of $G\alpha_O$ -associated protein complex. We first ensured that this Co-IP screening detected the beta subunits of G-binding protein (GNB1, 2, and 4) in the co-purified complex (Figure 1B). On the contrary, we found that the $G\alpha_O$ complex contained cytoskeleton-related proteins, such as spectrin and ankyrin. A bioinformatic analysis with Gene Ontology Consortium (http://www.geneontology.org/) revealed that the functional categories of "pre-mRNA binding," "actin filament capping," and "cortical cytoskeleton" were significantly enriched in the $G\alpha_O$-binding proteins (Figure S1B).

Of note, another DEE-associated protein SPTAN1 (spectrin alpha non-erythrocytic 1, Figure 1B) was predicted to form a protein complex with $G\alpha_O$. We validated the complex formation with a Co-IP assay using the extracts from Neuro2a cells (Figure 1C). Because we were unable to pull-down endogenous $G\alpha_O$ with the commercial anti-$G\alpha_O$ antibodies, we used anti-GFP for validation assays with Neuro2a cells. Immunofluorescence studies showed that endogenous $G\alpha_O$ and SPTAN1 proteins were co-localized in the cytosolic and peri-membranous regions of Neuro2a cells (Figure 1D). Intriguingly, $G\alpha_O$-positive Neuro2a cells co-expressed Sptan1 at higher levels than other cells.

Because Neuro2a is a mouse neuroblastoma cell line, we attempted recapitulating these data in more physiological models for human diseases. Specifically, we have reported that the direct conversion systems of neurons from human fibroblasts and stem cells in exfoliated deciduous teeth (SHEDs) are instrumental for investigating neurodevelopmental disorders.[29,36] Co-IP was unfeasible because the amount of total protein that can be recovered from these cells is too little for this assay. We therefore analyzed the colocalization signals of endogenous $G\alpha_O$ and SPTAN1 in these models, and the immunofluorescence data supported the co-expression of these two proteins (Figure 1E,F).

We have recently demonstrated that the expression of functionally related genes is coregulated in different tissues at a higher chance than those of unrelated genes.[24,26,37] We therefore tested this possibility in multiple lineages of human neuronal cells.[29,38] Quantitative polymerase chain reaction (qPCR) showed that the expression of *GNAO1* and *SPTAN1* mRNAs were robustly increased in induced neurons, by factors of 14 and 2.7, respectively, compared to fibroblasts before neuronal differentiation (Figure S2A). *GNAO1* was also highly expressed in dopaminergic neurons differentiated from mesenchymal stem cells in human deciduous teeth (Figure S2B).

These data prompted us to further examine the presence of endogenous protein complex containing $G\alpha_O$ and Sptan1 in the mouse brain. Although Co-IP was unattainable with anti-$G\alpha_O$ antibody, we alternatively used anti-Sptan1 antibody to perform Co-IP with the brain extract. Based on this method, we verified that the endogenous Sptan1-involving complex also contained $G\alpha_O$ in the postnatal mouse brain (Figure 1G). In agreement with these data, the murine homolog of $G\alpha_O$ was already expressed in the brain of wild-type C57BL/6 mice at embryonic day 16.5 (Figure S3A). Mouse Sptan1 was temporally and spatially co-expressed with Gαo in the postnatal murine brain (Figure S3B).

3.2 | Regulation of cytoskeletal remodeling by $G\alpha_O$

To clarify the functional relationship between $G\alpha_O$ and SPTAN1, we first attempted siRNA-mediated silencing of *Gnao1*, the murine homolog of *GNAO1*, which was endogenously expressed in Neuro2a cells (Figure 2A). We hypothesized that siRNA to *Gnao1* might also reduce the expression of *Sptan1* as a transcriptionally coregulated gene with *Gnao1*. However, the acute knockdown of *Gnao1* did not support this possibility under our experimental conditions (Figure 2A).

Immunofluorescence showed that the neurites in *Gnao1*-deficient cells were shorter in length (Figure 2B), but comparable in number compared with those in control cells (Figure 2C). Immunoblotting showed that knockdown of *Gnao1* did not affect the expression of full-length Sptan1; however, it increased the amount of cleaved product under resting conditions (Figure 2D). We therefore explored whether the loss of *Gnao1* ($G\alpha_O$) expression disturbed the molecular pathway associated with cytoskeletal remodeling. To this end, we analyzed the time course for the cleavage pattern of Sptan1 after treating the cells with 5 μM ionomycin, a potent activator of calcium ionophore and calpains.[39,40] We confirmed that 15 to 30 minutes of ionomycin treatments induced the cleavage of Sptan1 in the control cells, whereas such responses disappeared in *Gnao1*-deficient cells (Figure 2D,E).

Because the calpain-dependent cleavage of Sptan1 is known to be correlated with the activation of the extracellular-signal-regulated kinase (ERK) pathway,[40,41] we examined the phosphorylation status of Erk1/2 after ionomycin treatment. In control cells, phosphorylated Erk1/2 (p-ERK) signals showed 3.0-fold higher intensity after stimulation over

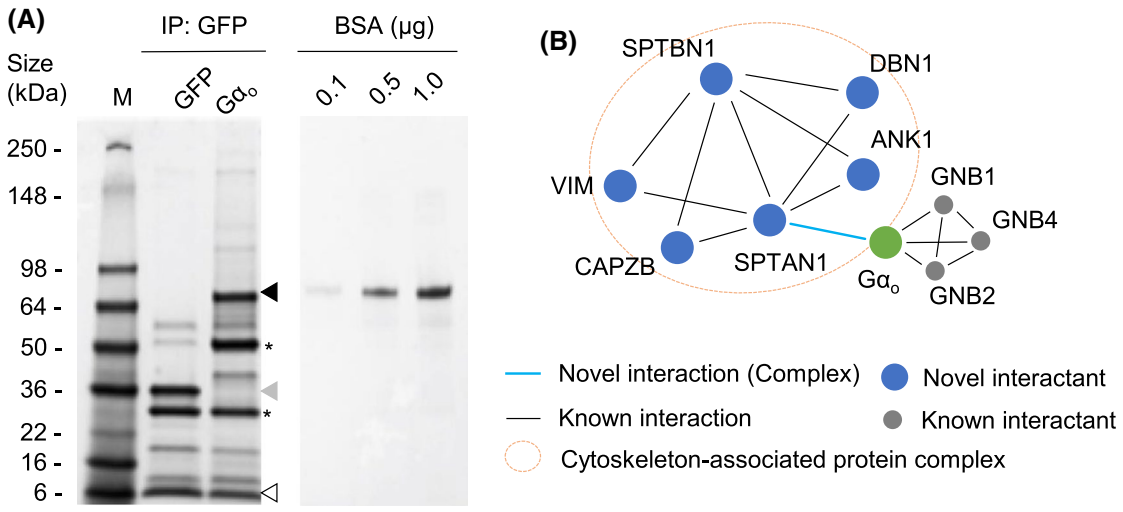

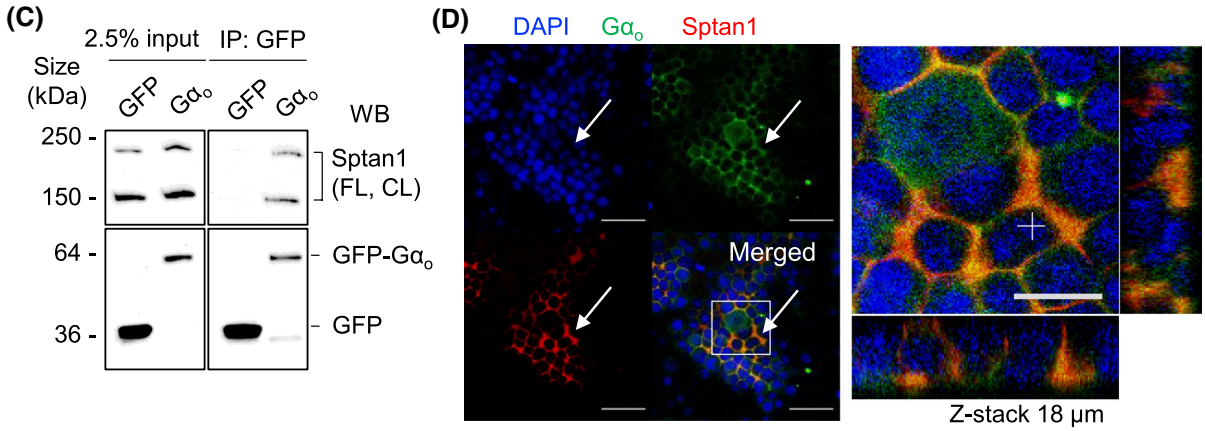

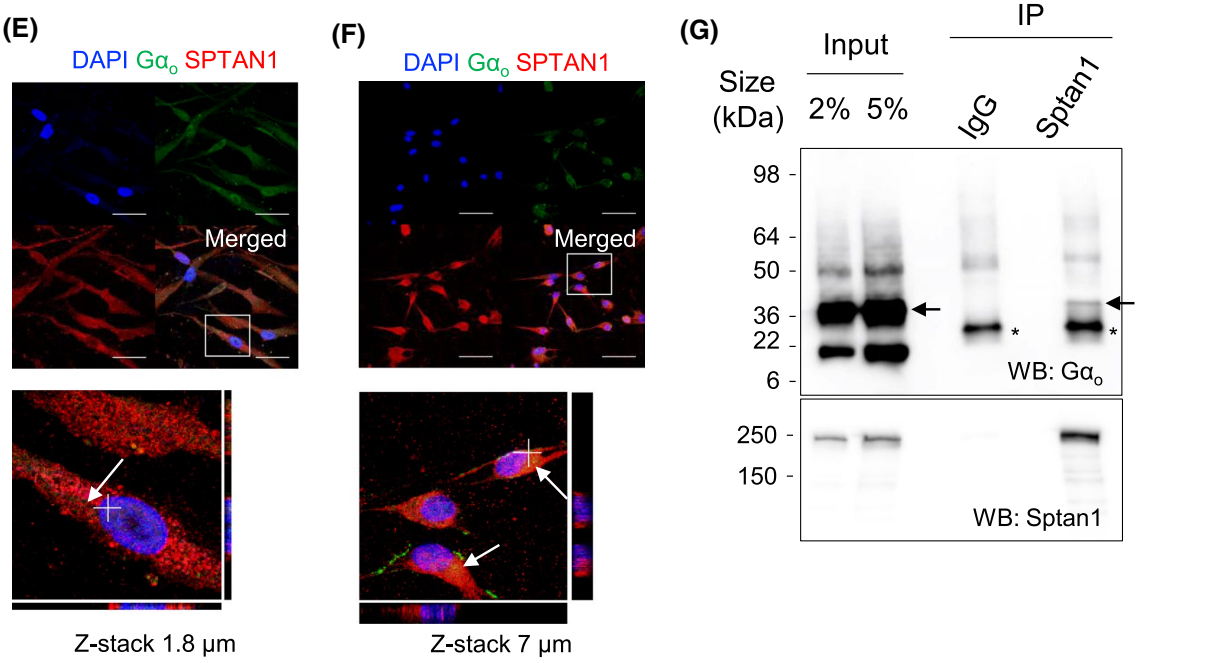

FIGURE 1 Interaction of $G\alpha_O$ with SPTAN1. A, SDS-polyacrylamide gel electrophoresis after co-immunoprecipitation with anti-GFP (JL-8). Protein standards (M, kDa) are shown on the left. IP lanes show the protein bands co-purified with GFP (negative control, lane 2) and $G\alpha_O$-GFP fusion protein (lane 3). Bovine serum albumin (BSA, lanes 4-6) shows the molecular size (67 kDa) and amount (0.1-1.0 μg/lane) of protein. Note that Coomassie Brilliant Blue detected 0.1 μg BSA. Black, gray, and white arrowheads indicate the $G\alpha_O$-GFP, GFP, and hemoglobin signals, respectively. Asterisks denote immunoglobulin heavy (50 kDa) and light (25 kDa) chains. B, A graphical summary of the interaction data. This study identified the cytoskeletal proteins as novel $G\alpha_O$-binding molecules (blue nodes in the dashed circle). The network highlights the interaction between $G\alpha_O$ and SPTAN1 (blue line) among previously known interactions (black lines) and proteins (gray nodes). C, Co-IP and Western blotting for validating the $G\alpha_O$-SPTAN1 interaction. Input lanes show Neuro2a extracts containing GFP (lane 1) and $G\alpha_O$-GFP fusion protein (lane 2). Sptan1 signals are present in the IP lane of $G\alpha_O$-GFP (lane 4) but not in GFP (negative control, lane 3). D, Co-localized signals of endogenous $G\alpha_O$ (green) and Sptan1 (red) proteins in Neuro2a cells. Arrows indicate the merged signals in cells expressing a low level of $G\alpha_O$-GFP. Scale bar, 50 μm (inset 20 μm). For D-F, squares denote the regions of interest for higher magnification. The cross signs point at the targets of optical sections for XZ (bottom) and YZ (right) images. E, Co-expression of $G\alpha_O$ and SPTAN1 in neurons directly converted from human fibroblasts. Arrows indicate the cells expressing both $G\alpha_O$ and SPTAN1. Scale bar, 50 μm. F, Co-expression of Gαo and SPTAN1 in dopaminergic neurons differentiated from human stem cells in exfoliated deciduous teeth. Scale bar, 50 μm. G, Validation of the endogenous protein in the mouse brain at 6 weeks of age. Representative data from Co-IP with anti-Sptan1 and immunoblotting for indicated proteins. The arrows indicate $G\alpha_O$ (40 kDa) and asterisks show the light chain (25 kDa)

the basal level (Figure 2D,E). In contrast, siRNA-mediated silencing of *Gnao1* disrupted the increase in p-Erk signals after the stimulation (median 42% of the control). These data indicated that Gαo plays an important role in ionomycin-induced cleavage of Sptan1.

As a GTP-binding protein, $G\alpha_O$ is considered to regulate not only ERK, but also various calcium-dependent signals in cooperation with phospholipase C (PLC). However, it remains unknown whether the loss of $G\alpha_O$ expression in neuronal cells results in the overactivation or the suppression of calcium-dependent molecular signals remains unclear.[9] Because the binding of AP-1 transcription factors to promoter regions reflects the activity of calcium-dependent signals,[42] we characterized the signaling condition of siRNA-transfected Neuro2a cells using the AP-1 promoter-driven luciferase reporter.[35] As expected, si*Gnao1*-treated cells showed 56% lower AP-1 activity than control cells at the resting condition ($P = .014$, Figure 2F, left), whereas the overexpression of the wild-type (WT) $G\alpha_O$ induced 2.5 times higher AP-1 activity than in nontransfected cells at the resting condition ($P = .014$, Figure 2F, right). The AP-1 activity was not increased during the observation period (6 hours after the ionomycin treatment) in either the si*Gnao1* or control group.

We further monitored the calcium influx before and after ionomycin stimulation using the fluorescence-based indicator Fluo4/AM.[43] In agreement with the data obtained in the luciferase assay, si*Gnao1*-treated cells showed a 28% lower calcium level before ionomycin treatment than the control cells ($P = .0043$, Figure 2G). Upon stimulation, the Fluo4/AM signal peaked more slowly in si*Gnao1*-treated cells than in control cells (7.7 seconds vs 2.6 seconds, respectively; $P < .001$) and showed an earlier decay after the peak (25% decay at 145 and 230 seconds, respectively; $P < .01$). The overexpression of mutant $G\alpha_O$ (G203R) did not show dominant-negative effects on the AP-1 promoter activity (Figure 2F, right) or ionomycin-provoked activation of the calcium signals (data not shown).

In addition, we explored whether or not DEE-associated mutant $G\alpha_O$ show impairments in the cleavage of Sptan1 after the ionomycin treatment and the complex formation with Sptan1 in Neuro2a cells. However, the overexpression of G203R, D174G, del191-197, and I279N proteins did not disturb the cleavage of Sptan1 (Figure 2H). Repeated Co-IP experiments did not support the possibility that mutant proteins were incapable of binding to the Sptan1 complex, either (Figure S4).

Given the regulatory role of $G\alpha_O$ in cytoskeletal remodeling, we examined whether or not this protein is responsible for activating morphogenic signals, such as Wnt pathway. However, we were unable to determine whether or not *Gnao1* regulates the canonical Wnt signal after the ionomycin treatment (Figure S5A,B). To gain further evidence that *Gnao1* organizes the morphogenic signals in vivo, we microinjected morpholino antisense oligonucleotides into the post-fertilized eggs of zebrafish to knockdown the *Danio rerio* homolog of *GNAO1* (*gnao1*). We found that zebrafish treated with the morpholino showed body axis anomalies at a significantly higher rate than control zebrafish (74% vs 18%, $P < .0001$, Chi-square's test; Figure S6). Notably, 28 of 60 (47%) *gnao1*-knockdown embryos showed impaired mobility during days 0-7 postfertilization, whereas only 11 of 103 (11%) control embryos presented with this motor phenotype ($P < .0001$). These data suggested that depletion of *gnao1* expression caused broad neurological dysfunctions in vivo, as observed in affected patients.[9,10]

3.3 | Establishment of GNAO1-knockout iPS and organoids

To investigate the pathogenic mechanisms of *GNAO1* encephalopathy in the human brain, we manipulated induced pluripotent stem (iPS) cells to make a new disease model of DEE (Figure S7A-E). MRI studies for patients with

GNAO1-associated DEE generally show normal appearance of lamination in the cerebral cortex,[9,10] suggesting that mutations in *GNAO1* have little effect on neurogenesis and the radial migration of neuronal progenitors. Thus, impaired neural connectivity, rather than the morphological defect of *GNAO1*-deficient neurons, might explain the molecular pathogenesis of this disorder. We considered such disorganized structure to be detectable in the brain-mimicking 3D

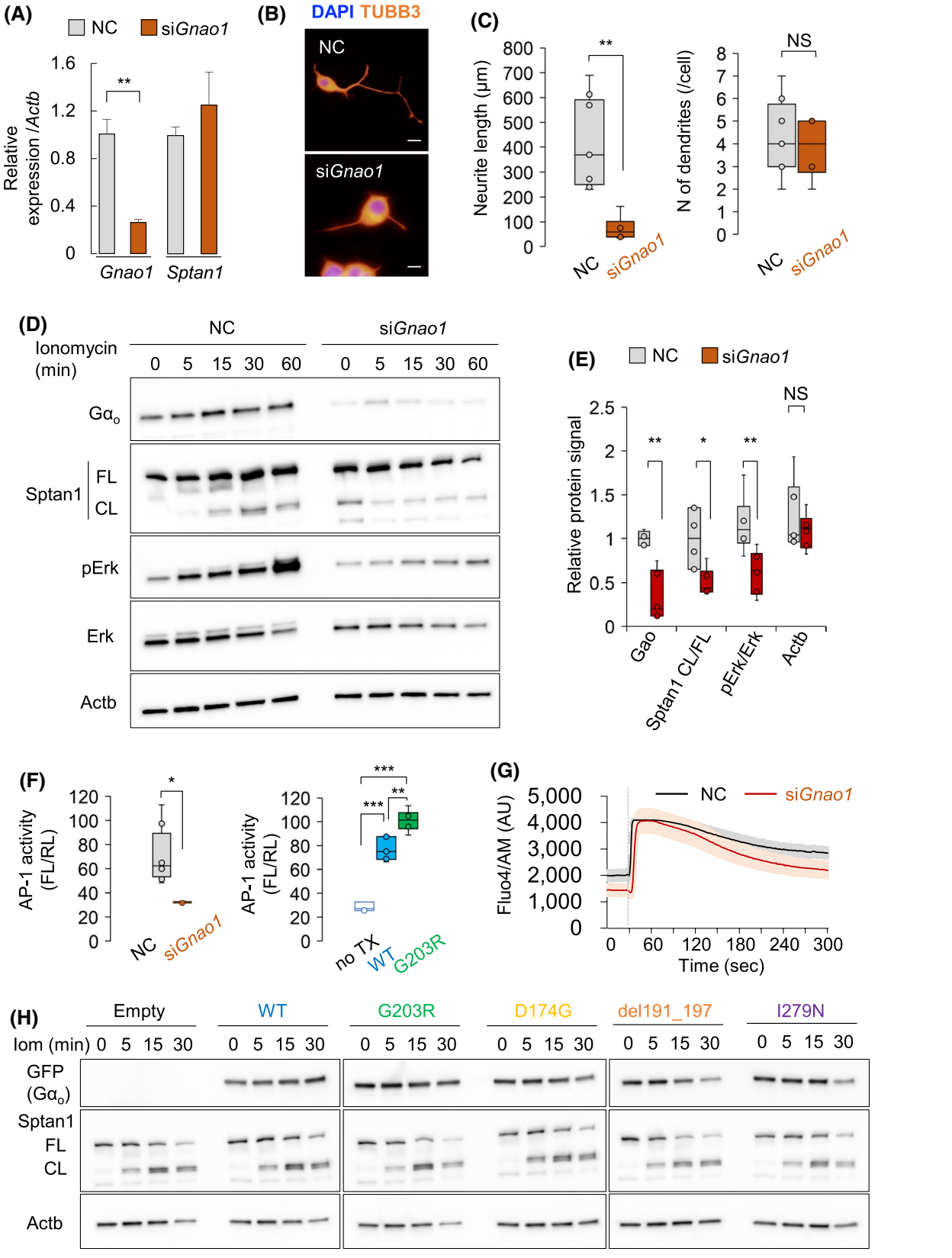

FIGURE 2 Knock-down of *Gnao1* homologs causes aberrant molecular signals. A, siRNA-mediated silencing of *Gnao1* in Neuro2a cells. Bar plots (mean ± SD, n = 4 each) show endogenous *Gnao1* and *Sptan1* mRNAs normalized to *Actb*. $^{**}P < .01$ (Student's *t* test). B, Microscopic images of Neuro2a cells treated with negative control (NC) or siRNA to murine *Gnao1* (si*Gnao1*). Scale bar, 50 μm. C, Box plots indicate the mean neurite length (μm/cell) and the number of neurites per cell of si*Gnao1*- or negative control-treated Neuro2a cells. $^{**}P < .01$ (Student's *t* test, n = 9 and 6 in control and si*Gnao1*, respectively). D, Time course of molecular signals after ionomycin treatment. Extracts from NC or si*Gnao1*-treated Neuro2a cells were subjected to Western blotting. The expression of the indicated proteins was analyzed at 0-60 minutes after 5 μM ionomycin treatment in a single blotting. The re-probed membrane shows the full-length form (FL, 250 kDa) and the cleaved product (CL, 150 kDa) of Sptan1. E, The relative signal intensity of each protein at 15 and 30 minutes after the ionomycin treatment was quantified and box-plotted (n = 6 from three independent experiments). $^{*}P < .05$, $^{**}P < .01$ (Student's *t* test). F, Left, 3xAP-1 luciferase reporter activity in Neuro2a cells transfected with control (NC) or *Gnao1*-silencing siRNA (*siGnao1*). Right, 3xAP-1 luciferase reporter activity in Neuro2a cells transfected with the wild-type (WT) or G203R mutant $G\alpha_O$-expression plasmids. Nontransfected cells (Non-Tx) were used as a reference. Renilla luciferase (RL) was used for internal control. $^{*}P < .05$, $^{***}P < .001$ (Student's *t* test). G, Fluo4/AM signals after 5 μM ionomycin treatment. The si*Gnao1*-pretreated Neuro2a cells show a lower calcium concentration at the resting condition, slower response to ionomycin, and earlier decay after the peak than those in control cells (NC). The vertical line at 30 seconds shows the time of ionomycin stimulation. Solid lines and shaded areas indicate the mean values and standard errors, respectively (n = 10 in each group). H, A representative Western blot for Neuro2a cells expressing WT and mutant $G\alpha_O$ proteins. In each group of transfection, the Gao, Sptan1 (FL and CL), and Actb expression are shown with the time course (0-30 minutes) after ionomycin (Iom) treatment

culture system of neurons, namely "cerebral organoids".[44] We reasoned that conventional monolayer neurons might partly recapitulate their subtle difference in morphology, and that combined analyses of monolayer neurons might compensate information at a single-cell resolution more efficiently than using only organoids.

We first established healthy adult-derived iPS cells and inactivated the endogenous *GNAO1* gene with the CRISPR-Cas9 system (Figure 3A and Figure S5F). Sequencing, immunofluorescence, and immunoblotting studies confirmed the absence of $G\alpha_O$ expression in 3 independent knockout (KO) cell lines (Figure 3B,C and Figure S5F). Using the standard protocol,[33] we ensured that both WT and *GNAO1*-KO iPS cells formed spheroids by 4 to 5 weeks of differentiation in vitro (DIV) (Figure 3D,E). We confirmed that the expression of $G\alpha_O$ was never recovered in KO cells (Figure 3C).

We found that KO spheroids showed an anomalous appearance with thin, bulbar structures on the surface (KO, Figure 3D). Patient-derived spheroids (G203R) appeared to be grown more slowly than WT and KO because they showed smaller size in diameter at 14 days of DIV (Figure 3E). Immunofluorescence studies showed that both WT and *GNAO1*-knockout spheroids expressed the differentiation markers for neuro-progenitor cells (NES), mature neurons (TUBB3), and cortical neurons (EMX1, FOXG1, TBR1, and Reelin) (Figure S8). However, when we observed the internal structure of KO and patient-derived spheroids at a higher magnification, they presented decreased expression of PAX6 and the aberrant pattern in gradient signals of NES signals (Figure 3F and Figure S8).

The expression of *PAX6*, *TUBB3*, *RELN,* and *TBR1* mRNAs was increased during the first 5 weeks of differentiation. However, their expression in WT and KO spheroids was indistinguishable during this period (Figure S9A). Similarly, the absence of *GNAO1* did not affect the expression profiles of other DEE-associated genes (*CDKL5*, *KCNT1*, and *SCN1A*) (Figure S9B). In contrast, KO spheroids expressed significantly lower levels of cytoskeleton-associated genes (*DBN1*, *GNB1*, and *SPTAN1*) than WT spheroids (Figure 3G). Because these genes encoded proteins that had been shown to be involved in the $G\alpha_O$-associated complex in this study, the qPCR data suggested that expression of $G\alpha_O$ and other molecules in the network (Figure 1B) might be coregulated in the developing neurons.

3.4 | Abnormal structure of GNAO1-knockout and patient-derived organoids

We continued to observe the development of WT, KO and the patient-derived (PT, G203R) organoids for longer periods (4 weeks and 35 weeks) until they formed the laminar and polarized structure of differentiating neurons. Compared to the organoids in the literature, these organoids showed immature lamination with few rosette formation.[45-47] Nonetheless, WT organoids continually expressed the progenitor marker, PAX6, while they began to show the surface layer expressing the mature neuronal marker, TUBB3, from 4 weeks of DIV (Figure 4A). On the contrary, KO and PT organoids showed decreased PAX6 signals in their deep layer at this age. When grown up for 35 weeks or longer, WT organoids were enriched with the expression of mature neuronal marker, NeuN, in broad areas (Figure 4B). The immature cells formed the meshwork signal of radial glial marker, GFAP, at the surface of WT organoids. Consistently, KO and PT organoids showed the GFAP signals at the superficial layer. However, they expressed higher levels of GFAP signals than WT, and appeared to perturb the differentiation of NeuN-positive neurons in the surface layer. These data suggest that both KO and PT organoids have common defects in the acquisition of polarized structure of progenitors and differentiating neurons,

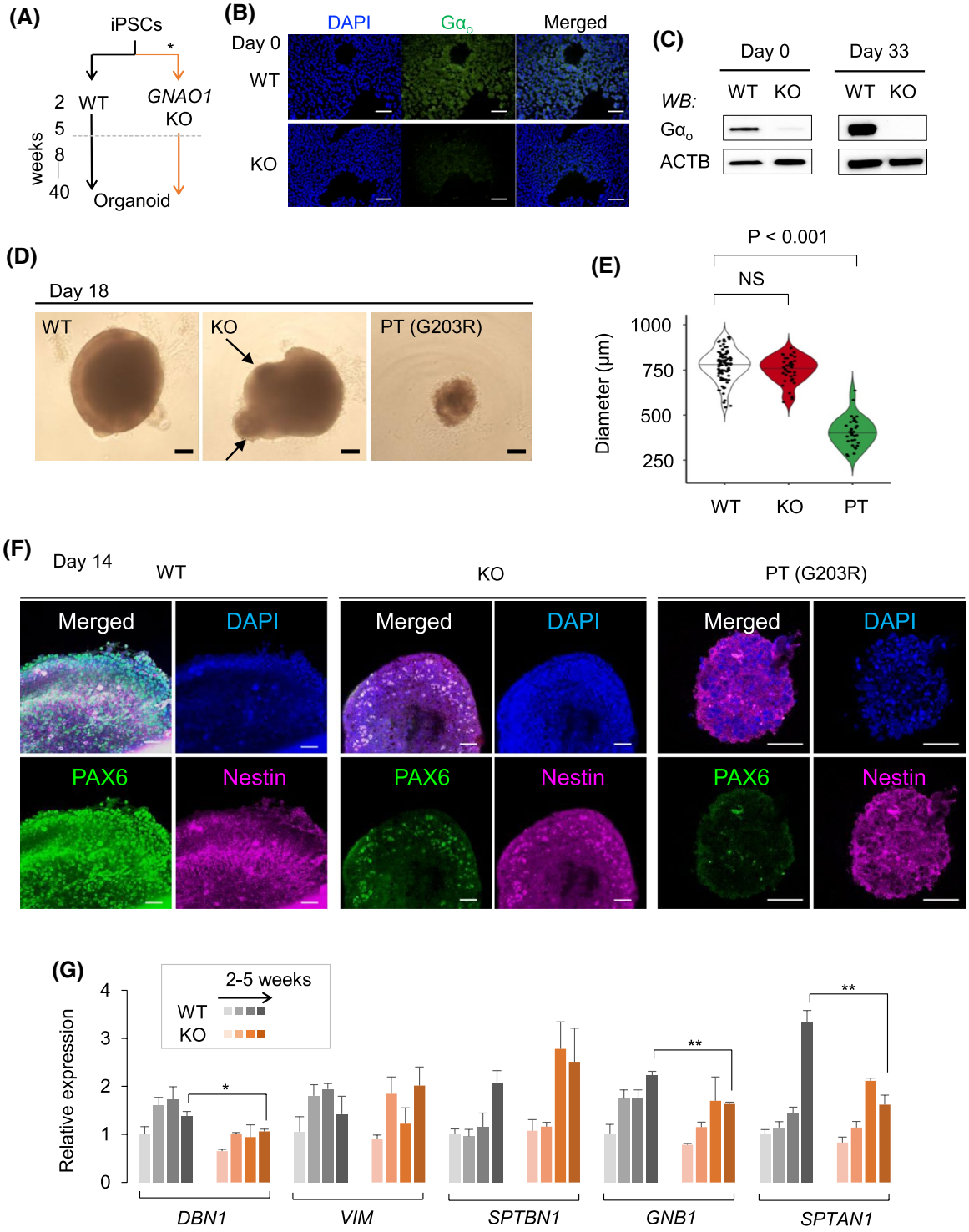

FIGURE 3 Establishment of *GNAO1*-knockout iPS cells and differentiation of neuro-spheroids. A, Workflow of the spheroid culture from iPS cells with or without inactivation of *GNAO1* by CRISPR/Cas9. The organoids in this study were mature spheroids after 15 weeks of differentiation. B, Immunofluorescence images of WT and *GNAO1*-knockout (KO) iPS cells. Scale bar, 150 μm. C, Western blotting for the whole extracts from WT and KO iPS cells at the indicated time (days) of differentiation. D, The dysmorphic appearance of KO and patient-derived (PT) spheroids at the early phase (18 days) of differentiation in vitro. Scale bar, 100 μm. E, The size (maximal diameter, μm) of WT (white), KO (red) and PT (green) spheroids at 18 days. Violin plots show median and distribution of each value (n = 32 in each group). F, Immunofluorescence images of WT, KO, and PT spheroids at 14 days. KO and PT spheroids expressed comparable level of NES but lower level of PAX6. Scale bar, 50 μm. G, The expression of mRNA encoding the $G\alpha_O$-binding proteins was significantly lower in KO spheroids than in WT spheroids at 5 weeks of differentiation. The data are shown as the mean ± SD (n = 3 for each group). *$P < .05$, **$P < .01$, and NS, $P > .05$ (Student's *t* test)

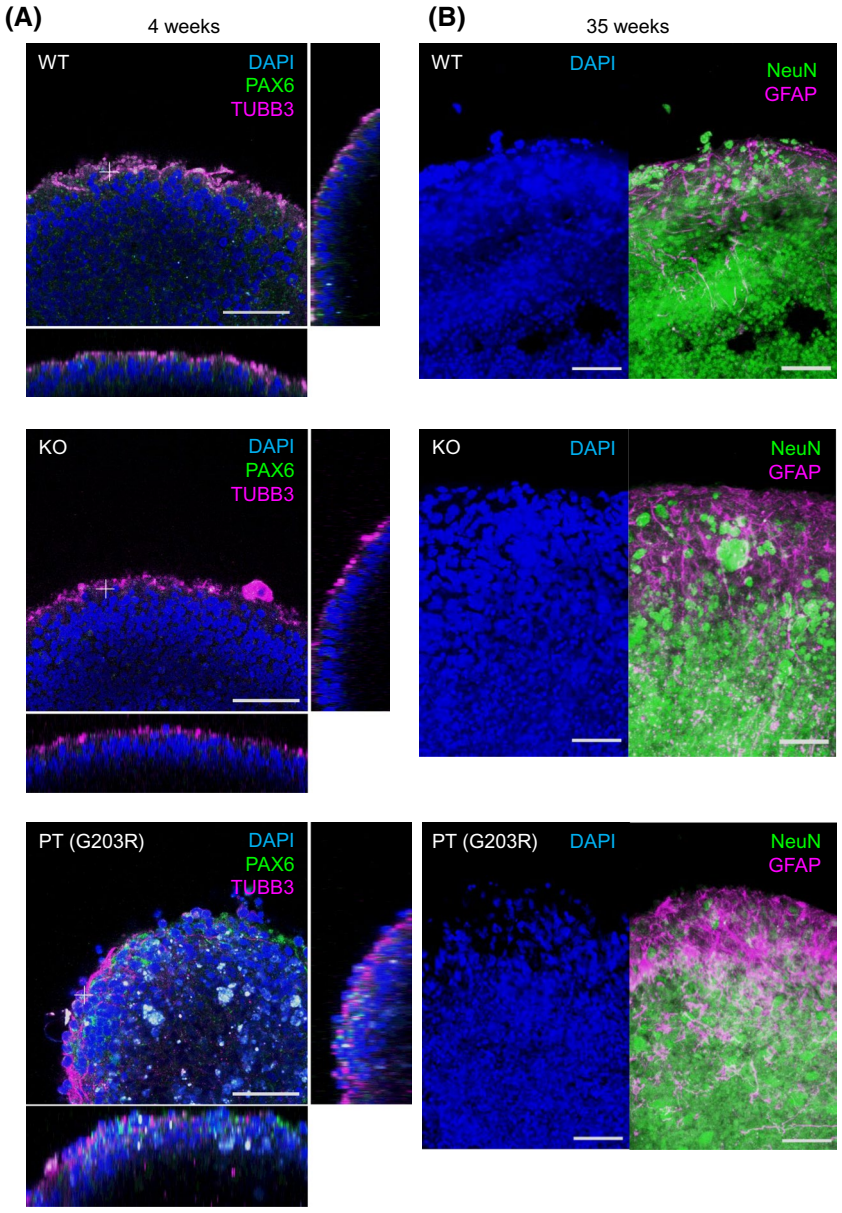

FIGURE 4 The fine assessment of the internal structure of WT, knockout and patient-derived neurons. A, Organoids at 4 weeks show diffusely distributed PAX6 (green) and gradient-expressed TUBB3 (magenta) signals. Cross signs indicate the targets of XZ and YZ sectioning. Scale bar, 50 μm. B, Organoids at 35 weeks developed the diffuse NeuN-positive neurons and the immature layer of GFAP -positive progenitors on surface (magenta). Scale bar, 50 μm

whereas the ability of KO and PT organoids to populate terminally differentiated neurons were not severely affected.

3.5 | Aberrant neurite outgrowth of GNAO1-disrupted neurons

To verify that the dysmorphic appearance of KO spheroids results from their functional deficits in organizing the cytoskeleton, we analyzed the internal architecture of WT and KO spheroids. In WT spheroids, the SPTAN1, SPTBN1, and TUBB3 signals showed a radially filamentous pattern on the surface (WT1) but not in the deep region (WT2) at 56 days of differentiation (Figure S10A). In contrast, KO spheroids did not show such ordered signals of cytoskeletal proteins in either region (Figure S10B). We also found that the KO neurons showed only faint signals of SPTAN1 both at the surface and in the deep layers of spheroids, recapitulating the enhanced cleavage of Sptan1 due to *Gnao1* depletion in Neuro2a cells (Figure 2D).

To characterize the morphological features of KO and patient-derived (PT) neurons at a single-cell resolution, we plated the spheroids on a laminin-coated dish from 5 weeks of differentiation. In this experiment, we noted that the attached neurons started extending neurites to adjacent neurons within 1 week (Figure 5A,B). Compared with WT neurons, the KO spheroids did not show a significant difference in the number of neurites or the neurite length (Figure 5C-E) but did show a significantly higher curve index of neurites ($P = .0006$, Student's t test; Figure 5F). Notably, PT neurons had not only shorter length of neurites, but also higher values of curve index than WT and KO neurons ($P < .001$). At a higher magnification, KO neurons presented with punctate signals of SPTBN1 in soma, suggesting that the reduced

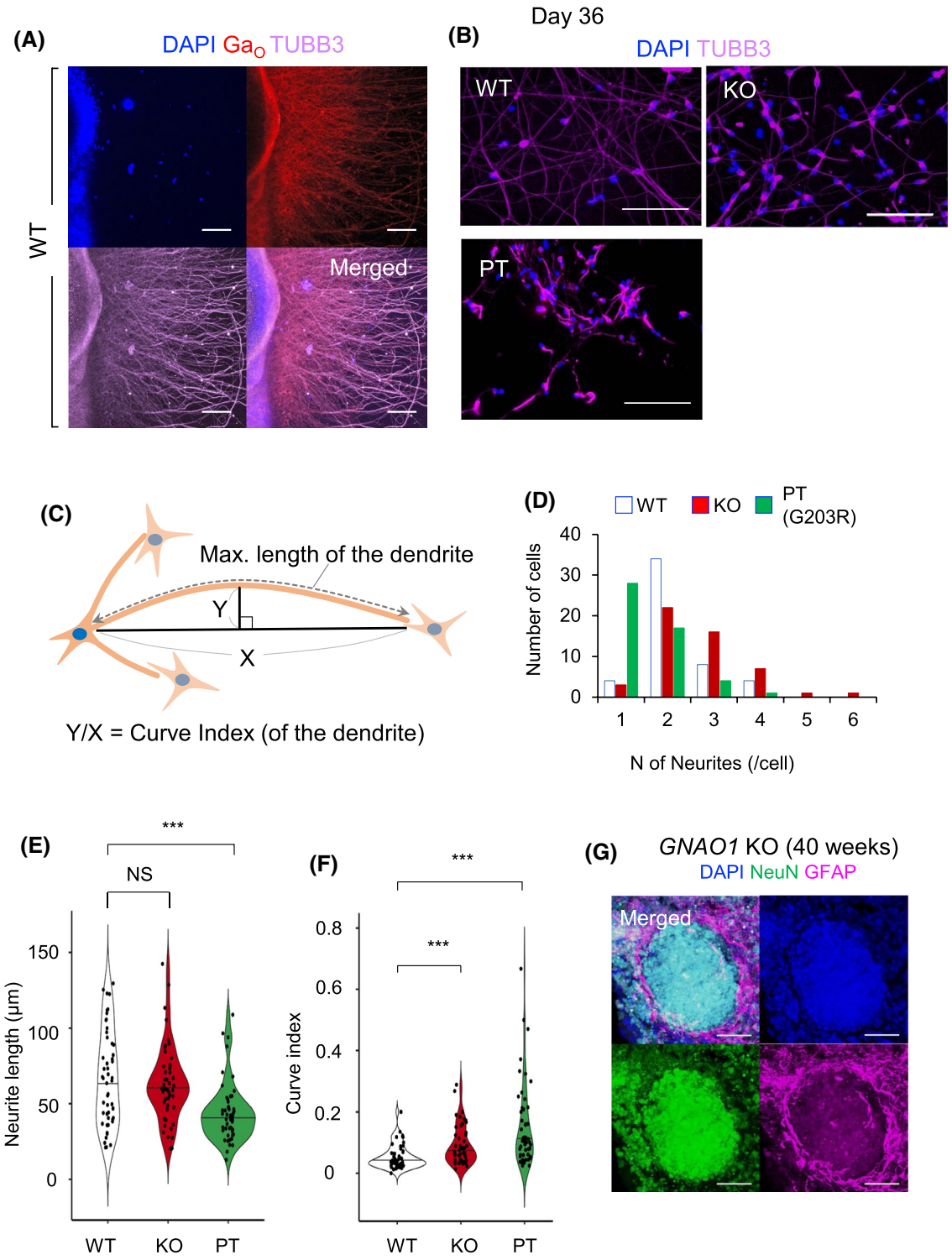

FIGURE 5 Morphological analysis of WT, knockout and patient-derived neurons. A, Confocal images of extending neurites from the surface of WT spheroid. After one week of culture on Laminin-coated cover glass, the whole spheroids were subjected to immunofluorescence without cryo-sectioning. Indicated proteins (Gα_O and TUBB3) were immunolabeled, and nuclei were visualized with DAPI. Scale bar, 100 μm. B, Dendritic outgrowth of neurons from WT, KO, and patient-derived (PT, G203R) spheroids. The neural networks of extended neurites are visualized as TUBB3-positive signals. Scale bar, 100 μm. C, An expository scheme for the measurement of the length (dashed lines) and "Curve Index" of a dendrite with the formula [Y/X]. This neuron has five dendrites. D, Histograms show the number of neurites per cell. E, Violin plots for maximal length of neurites (μm). F, Violin plots for curvature index of neurites. ***$P < .001$ (Student's t test). NS, not significant. G, An aggregated clump of NeuN-positive neurons (green) surrounded by the GFAP-positive fibers (magenta) in KO organoids at 250 days of differentiation. Scale bar, 50 μm

expression of SPTAN1 left unbound aggregates of endogenous SPTBN1 (Figure S11).

In agreement with the dysmorphic feature of monolayer neurons, the *GNAO1*-KO organoids were found to form globular clumps of NeuN-positive neurons surrounded by the GFAP-positive, immature progenitors (Figure 5G). These data therefore indicated that the "bulbar structure" of spheroids at 14-18 days reflects the cellular phenotypes KO neurons (Figure 3D), which was partly associated with incomplete acquisition of neuronal differentiation.

3.6 | GNAO1 regulates the expression of Ankyrin G

Because KO spheroids showed a lower expression of SPTAN1 than WT at both the mRNA and protein levels (Figure 3G, Figures S10 and S11), we wondered whether the loss of *GNAO1* might cause functional deficits in the process of axonal initial segment (AIS) formation.[48-50] WT spheroids expressed 2.9- and 45-fold higher levels of *KCNQ2* and *ANK3* mRNA, respectively, at 5 weeks of differentiation than at 2 weeks. KO spheroids, in contrast, were incapable of inducing these genes at the WT level during this period of differentiation (Figure S12A,B). The expression of *SPTBN4* was not significantly affected in KO spheroids (Figure S12A), excluding non-specific effects due to the disruption of *GNAO1*.

By 4-5 weeks of differentiation, however, immunofluorescence studies never detected a valid signal of Ankyrin G (AnkG). Repeated experiments indicated that spheroids at more than 15 weeks of differentiation (>100 days of age) began to show the rod-shaped signal of AnkG (Figure S13A). We therefore defined mature spheroids as "organoids" when immunoreactivity to AnkG proved positive in axons. In contrast, we never detected AnkG signals in KO spheroids (organoids), even beyond 15 weeks of differentiation. To confirm the depleted expression of AnkG in mature KO organoids, we further extended the period of differentiation to ≥52 weeks (1 year) of differentiation.

During the extended period of organoid differentiation, we also established another iPS cell line from a girl harboring a p.G203R mutation in *GNAO1*.[10] The established iPS cells passed the same quality tests as WT and KO iPS cells. We therefore prepared the patient (PT)-derived organoids in parallel with WT and *GNAO1*-KO organoids at >40 weeks of differentiation for the morphological analysis. Because these mature organoids had grown up to 3.5 mm in diameter, we applied the "Scale" method[51] to obtain the deep-layer signal of immunofluorescence (Figure 6A). WT organoids exhibited a smooth, spherical appearance, even at this age, whereas KO and PT (G203R) organoids showed an anomalous structure (Figure 6B). The internal structure of WT organoids showed the extension of TUBB3-positive neurites, whereas KO and PT (G203R) organoids lacked such an orderly architecture (Figure 6C). We further confirmed that KO and PT (G203R) organoids expressed AnkG at significantly lower levels than the WT organoids ($P < .001$, Student's t test; Figure 6C,D and Figure S13B). The immunofluorescence studies also revealed that PT (G203R) organoids expressed TUBB3 at significantly higher levels than WT and KO organoids (Figure 6C,D), possibly due to its different genetic background. Alternatively, the dominant-negative effects of the *GNAO1* mutation (G203R) on cytoskeletal remodeling might have led to a compensatory increase in the TUBB3 expression. qPCR showed that the expression of *ANK3* (AnkG-encoding mRNA) did not differ markedly between WT and KO organoids at this age (Figure S13C). It was therefore suggested that the deficient signals of AnkG might be due to a reduced translational efficiency or decreased protein stability in KO and PT (G203R) organoids compared with those in WT organoids.

We further tested whether the KO and PT (G203R)-derived monolayer neurons showed reduced expression of AnkG. Quantitative measurement of immunofluorescence signals confirmed that they showed lower fluorescence signals of AnkG and $G\alpha_O$ than WT monolayer neurons ($P < .01$, Student's t test; Figure 6E).

3.7 | Impaired firing of GNAO1-KO neurons

To verify that deficient expression of $G\alpha_O$ causes impaired calcium signaling in developing neurons, we tested the reactivity of monolayer neurons to ionomycin. We analyzed the firing activity of neurons using Fluo4-based calcium imaging.[43] We used WT and KO organoids at 42-43 weeks (300 days) of differentiation because organoids younger than this did not respond to stimulation with ionomycin. We found that WT neurons rapidly responded to the stimulation and demonstrated synchronous firing from one side (region of interest [ROI] 1-4) to the other (ROI 5-8) (Figure 7A,B and Figure S14A). In contrast, KO neurons were substantially inert to the chemical stimulation.

The quantitative measurements of fluorescent signals showed that WT and KO organoids had a similar oscillating activity at the basal condition (0-20 seconds, Figure 7B,C). Upon stimulation at 20 seconds, Fluo4 signals of WT neurons reached the maximal intensity during 1-1.5 minutes (ROI 1 −4) and 2.5-3 minutes (ROI 5-8) of recording time. We confirmed that the maximal intensity was significantly higher than those of KO (381.1 ± 166.3 vs 36.1 ± 20.7 rfu, $P = 5.79 \times 10^{-4}$, Student's t test, Figure 7D). During the activation phase (2-5 minutes), WT neurons also showed significantly higher rate of firing than KO (0.91 ± 0.71 vs

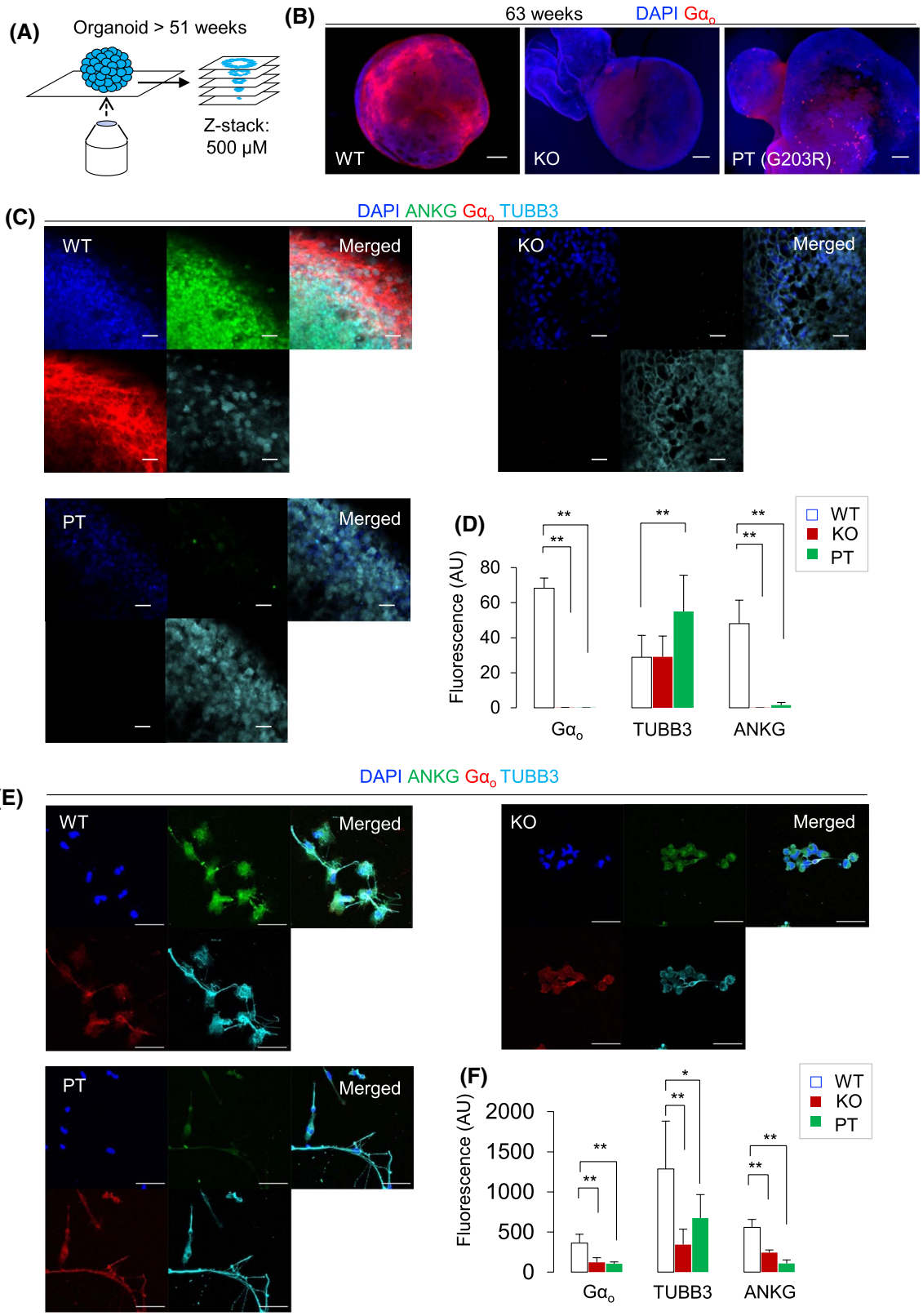

FIGURE 6 The deficient expression of the axon initial segment components in *GNAO1*-KO and patient-derived organoids. A, A Scale-pretreated organoid (>40 weeks of differentiation) mounted on a coverslip. A total of 150-200 optical sections (>500 μm in-depth) were reconstituted into Z-stack images. B, The general appearance of WT and *GNAO1*-mutant organoids. "G203R" is the organoid from a patient carrying a de novo p.G203R mutation in *GNAO1*. Scale bar, 50 μm. C, The absence of AnkG signals in KO and patient-derived (G203R) organoids. WT organoids show $G\alpha_O$- and AnkG-positive neurons at the surface and near-surface layers. Scale bar, 50 μm. D, Quantitated results of immunofluorescence signals in the panel C. $^{**}P < .01$ (n = 10 for each, Student's *t* test). E, AnkG, $G\alpha_O$ and TUBB3 signals in WT, KO, and patient (G203R) monolayer neurons. Scale bar, 50 μm. F, Quantitated results of immunofluorescence signals in the panel E. AU, arbitrary unit. $^{**}P < .01$ (n = 10 for each, Student's *t* test)

0.041 ± 0.058 times/min, $P = 1.06 \times 10^{-2}$, Student's t test, Figure 7E).

To clarify the molecular basis for the inefficient excitation of KO neurons, we characterized the gene expression profile of KO organoids by qPCR in comparison with WT (n = 4 for WT and KO). KO organoids expressed similar levels of P2X and P2Y purinergic receptors (mRNAs) to WT organoids (Figure S14B). Notably, the expression of

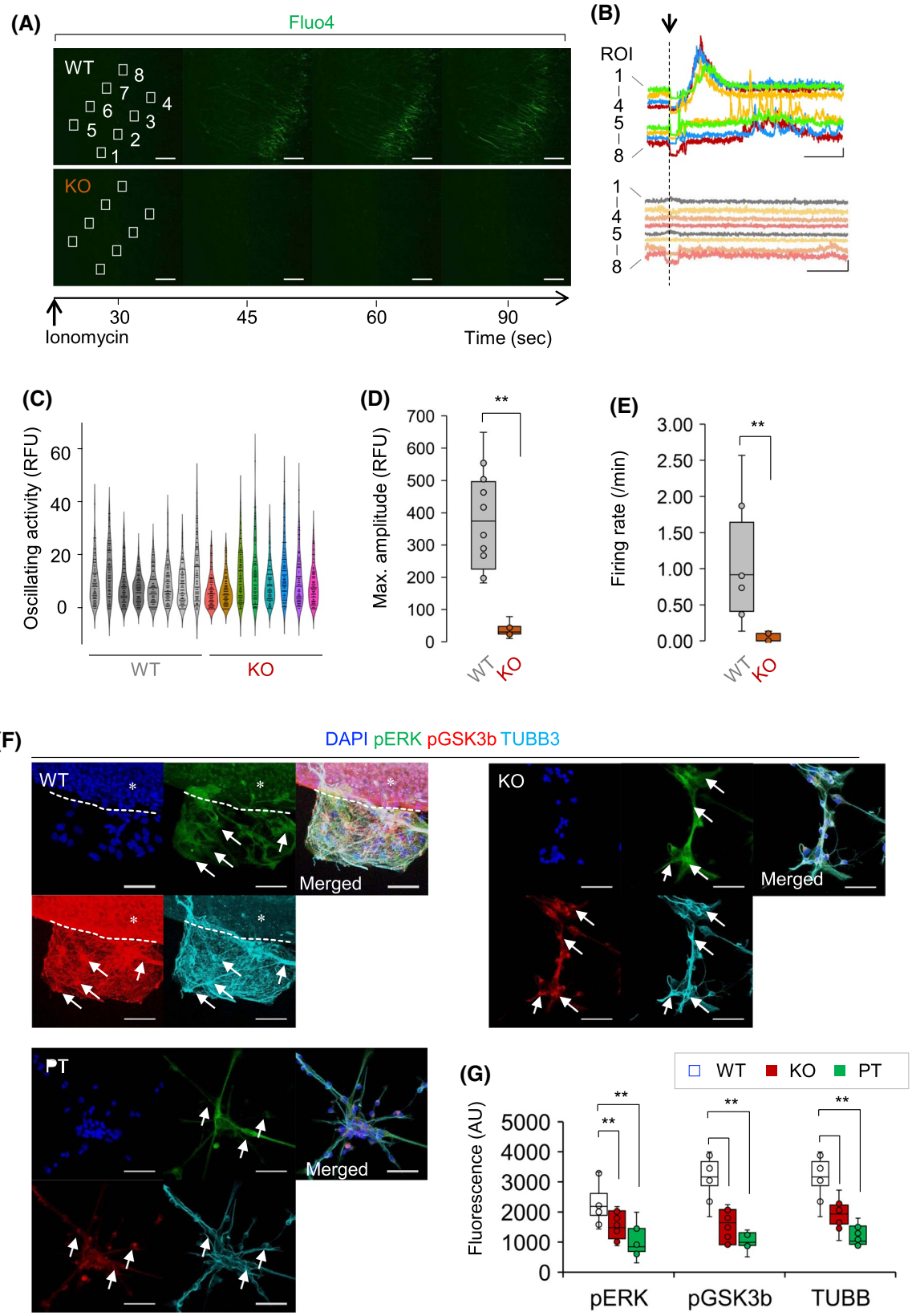

FIGURE 7 Defective firing and connectivity of *GNAO1*-KO neurons. A, Time-lapse imaging of Fluo4/AM signals. Panels show firing neurons (green) at the indicated time after stimulation with 100 μM ionomycin. For WT neurons, six regions of interest (ROIs, 1-4 and 5-8) are placed according to the direction of excitation. In KO neurons, the ROIs are set to the positions corresponding to those of WT neurons. B, Traces of Fluo4/AM signals in ROIs 1-8 of WT and KO neurons. The vertical lines indicate the time point of chemical stimulation. The scale indicates the duration (1 minute) and amplitude (50 relative fluorescence units [RFU]). C, Oscillating activity of WT and KO neurons at the basal condition (ROI 1-8 for each). D, The maximum fluorescence intensity (RFU) of WT and KO neurons after stimulation. E, Firing rate (spikes/min) of WT and KO neurons after stimulation. For D and E, $*P < .05$ (n = 8 in each group, Student's *t* test). F, Immunofluorescence signals of pGSK3b, pERK, and TUBB3 in WT, KO, and patient-derived (PT, G203R) monolayer neurons. The dashed line in WT indicates the edge of the organoid (*) located above the TUBB3-positive monolayer neurons (arrows). Immunofluorescence of organoid was not included in the quantitative analysis of fluorescence signals in G. Scale bar, 50 μm. G, Quantitated results of immunofluorescence signals in the panel F. AU, arbitrary unit. $**P < .01$ (n = 10 for each group, Student's *t* test)

the vesicular glutamate transporter 2 (VGLU2)-encoding gene *SLC17A6* in KO organoids was decreased to 44% of that in WT organoids ($P = .021$, Student's *t* test). Other presynaptic (*SYP* and *NRXN1*) and postsynaptic marker-associated genes (*DLG4* and *HOMER*) were normally expressed (Figure S14B). Canonical Wnt pathway-associated genes (*AXIN2*, *SEMA3A*, *L1CAM*, and *GJA1*) were expressed in KO organoids at 1.2- to 2.0-fold higher levels than in WT organoids ($P = .046$, .0040, .26, and .041, respectively, Student's *t* test; Figure S14B). These data indicated that the defect of *GNAO1* ($G\alpha_O$) expression in the developing brain caused impairment not only in single-cell firing but also in trans-synaptic neural connectivity due to altered molecular signaling, such as ERK and Wnt-GSK3β pathway (Figure 7F and Figure S12).

Lastly, to validate the differential activity of molecular signals in *GNAO1*-KO and patient-derived (G203R) monolayer neurons, we examined their p-ERK and pGSK3β signals under resting conditions. We found that KO and G203R neurons showed lower p-ERK and pGSK3β signals than WT (Figure 7F,G), suggesting that deficient expression of WT $G\alpha_O$ causes the impaired activation of calcium-dependent molecular signals in the developing brain (Figure S15).

4 | DISCUSSION

In this study, we identified SPTAN1 as a novel binding partner of $G\alpha_O$. Because these two proteins are both associated with DEE, we were particularly interested in the molecular pathway that might be commonly disturbed in the brain of affected children.[26,36] We first found that siRNA-mediated depletion in *GNAO1* disrupted the activation of molecular signals associated with the cleavage of SPTAN1. We also found that the loss of $G\alpha_O$-SPTAN1 interaction was correlated with inefficient cleavage of SPTAN1 after ionomycin treatment.

GTP-binding proteins are known to activate phospholipase C (PLC) in various tissues.[17] PLC has been also characterized as an essential molecule for organizing neurite outgrowth.[52] More recently, Go proteins were shown to link Wnt-Frizzled signaling to the functional development of neuromuscular junctions in *Drosophila*.[53] Thus, our data reproduced the previously established concept that $G\alpha_O$ regulates the morphogenesis and acquisition of cell polarity.[20,54,55] In agreement with this notion, a recent report showed clinical evidence that a decrease in PLC beta activity was associated with the pathogenic mechanisms underlying DEE.[56] Although our study did not identify PLC as an interacting molecule with $G\alpha_O$, we consider it valuable to investigate the formation of the $G\alpha_O$-PLC-SPTAN1 complex in the developing brain.[57] We did not identify the interaction of $G\alpha_O$ and PLC in our Co-IP study mainly because we used a mild condition for protein solubilization with 1% Triton-X. Membrane-bound phospholipases might be more efficiently recovered with different detergents, such as deoxycholate and 3-[(3-cholamidopropyl) dimethylammoniol-l-propanesulfonic acid (CHAPS).[58] Such research will help clarify whether or not PLC might cooperate with $G\alpha_O$ to link morphogenic signals with the functional differentiation of neurons in the developing brain.

It might be reasonable to hypothesize that the activation process depends on the interaction of $G\alpha_O$ with PLC-beta and subsequent synthesis of second messengers, regardless of its interacting profile with SPTAN1. However, adhesion of another cytoskeletal protein, actin, to the plasma membrane has been reported to occur in parallel with the activation of PLC and rapid turnover of phosphatidylinositol phosphates.[59] It is also noteworthy that transactivation of different molecular signals required the periodic assembly of skeletal proteins in association with membrane-bound receptor in axons and dendrites.[60] From this perspective, one could argue that $G\alpha_O$ interacts with SPTAN1 so that it comprises a membrane-bound complex that works as a platform for the efficient activation of calcium signaling (Figure S15).

The AIS, which sits at the base of the axon in mature neurons, forms a highly specific structure for the directional propagation of action potentials from the dendritic domain to the distal axon.[61,62] At the molecular level, scaffold proteins organize the layer structure of AIS spanning from microtubule to the plasma membrane.[63] Among them, AnkG plays a crucial role in the assembly of other scaffolding proteins, including SPTAN1, and ion channels at the dense compartment

of AIS.[64] Details regarding the developmental process of the AIS remain elusive; however, cortical neurons were shown to express AnkG at the proximal axon immediately after birth in mice.[48] Another murine model also showed evidence that the impaired assembly of Sptan1 in the AIS caused early-onset seizures and death within 1 month after birth.[49] The functional deficit of AIS has been recently implicated in the pathogenic mechanisms of DEE, as multiple DEE-associated proteins (voltage-gated channels) are highly enriched in the AIS.[65] Our findings suggest that $G\alpha_O$ might organize the functional connectivity of neurons in the postnatal brain by regulating the physiological development of the AIS.

The calcium imaging system revealed that (*GNAO1*)-KO neurons poorly responded to ionomycin treatment, although the spontaneous firing of KO neurons remained comparable to that of WT neurons under resting conditions. This result also highlights the alternative perspective that KO neurons were no longer able to transmit their excitation to adjacent neurons. This loss of the directional wave may possibly be due to the presence of an aberrant neuronal polarity.[66] We rationalized that these findings were consistent with the biochemical deficit of KO organoids for the expression of AnkG. Specifically, KO neurons failed to acquire functional polarity, which is necessary for generating valid action potentials and coordinated firing of neurons in the developing brain.[19,48,49] Previous studies showed that *GNAO1* plays a functional role in norepinephrine-induced calcium-current inhibition.[9] In our study, Gao was rather associated with the activation of the calcium influx and downstream signals in neuron. Although our data seemed to raise an opposing concept to previous studies, these data might imply that Gao regulates both positively and negatively the calcium-dependent signals in response to different types of stimulation.

We have no experimental evidence that clearly explains why *GNAO1*-KO organoids expressed lower *ANK3* mRNA levels in an early stage. In a later stage, they showed comparable mRNA expression but a lower expression of Ank-G protein. Given the impaired calcium-dependent signals in Neuro2a cells, we hypothesized that there might be time-dependent mechanisms by which *GNAO1*/Gao regulates in early and late stages of neuronal development. In the earlier stage of development, Gao turns on calcium-dependent signals and AP-1 activity, for example, thereby accelerating the transcription of SPTAN1 and ANK3 in proliferating progenitors. In the later stage, terminally differentiated neurons stop proliferation. Calcium-dependent signals in mature neurons may assume more responsible roles in the calpain-mediated cleavage and remodeling of cytoskeletal proteins, including SPTAN1 and Ank-G.[67] Calcium-dependent signals are established to regulate both transcription and cytoskeletal architecture in synaptogenesis,[42] while expression of SPTAN1 is upregulated in highly metastatic cancer.[68] We therefore considered the possibility that *GNAO1*/Gao regulates the expression of cytoskeletal molecules at the mRNA level and their stabilities at the protein level through calcium-dependent molecular signals.

The loss of dendro-axonal polarity in KO neurons may explain why patients with *GNAO1* encephalopathy develop such a broad spectrum of neurological phenotypes: intractable seizures, involuntary movements and cognitive impairments from early infancy.[10,11,69] KO organoids expressed a presynaptic marker *SLC16A7* (VGLU2) at a significantly lower level than WT organoids. We also observed the increased expression of other canonical Wnt signaling-associated genes (*AXIN2*, *SEMA3A*, *L1CAM*, and *GJA1)* in KO organoids. We are currently unable to confirm that these gene expression profiles are relevant to the neurodevelopmental phenotypes of *GNAO1* encephalopathy. However, patients with *GNAO1* encephalopathy might suffer from an impairment in the directional conductance of neural excitation due to the aberrant dendro-axonal polarity.

Limitation of this study may reside in the fact that we have not fully validated the cytoskeletal phenotypes and aberrant signals in organoids and their epileptogenic effects in vivo. Critical limitations may also include the lack of evidence that Gao and SPTAN1 directly interact with each other. Because we cannot exclude the possibility that the third proteins may mediate their interaction in one complex, we need to perform further experiments with yeast-two-hybrid or cell-free purified system for solving this question. Because Neuro2a cells and brain organoids showed inconsistent phenotypes in their neurite outgrowth and the protein stability of the p.G203R mutant, these data must be qualified in further experiments using the patient-mimicking knock-in mice. We have not determined whether or not calcium-dependent signals coregulate the expression of the two DEE-associated proteins $G\alpha_O$ and SPTAN1, in organoids. An unsupervised transcriptomic approach may clarify the presence or absence of such molecular signals in the developing brain. Identifying the molecular targets for normalizing the cytoskeleton-associated signals will also open a new venue for discussing the potential for future translational research along this concept.

In conclusion, we showed that *GNAO1* ($G\alpha_O$) organizes the functional connectivity and synergic firing of neurons in the developing "mini-brain." The loss of $G\alpha_O$ expression resulted in the deficient expression of AIS-constituting proteins (SPTAN1 and AnkG), suggesting the potential role of $G\alpha_O$ in the acquisition of neuronal polarity. Correcting the $G\alpha_O$-AIS axis might be a therapeutic target in the future for patients with DEE of various causes.

ACKNOWLEDGMENTS

We thank the patients and their parents for kindly cooperating with this study; Drs. Toshiro Hara (Fukuoka Children's Hospital) and Kazuaki Nonaka (Professor Emeritus, Kyushu University) for cordial supports of this research; Dr Huda

Y Zoghbi (Neurological Research Institute, Texas) for the critical review of this manuscript; and Dr Brian Quinn for proofreading this manuscript. This study was supported by JSPS KAKENHI grant numbers 19K08281, (Y. Sakai), 18H04042 (T.A. Kato), 18K07821(Y. Ishizaki) and 17H01539 (N. Matsumoto); AMED under the grant numbers JP19ek0109411/JP20ek0109411, JP20wm0325002, JP19ek0410039 (Y. Sakai), JP20ek0109486, JP20ek0109348, JP20kk0205012 (N. Matsumoto); a Health and Labour Sciences Research Grant (N. Matsumoto), that on Evidence-based Early Diagnosis and Treatment Strategies for Neuroimmunological Diseases from the Ministry of Health, Labour and Welfare of Japan (Y. Sakai); Life Science Foundation of Japan (Y. Sakai); Takeda Science Foundation (Y. Sakai, N. Matsumoto); The Mother and Child Health Foundation (Y. Sakai), The Japan Epilepsy Research Foundation (Y. Sakai), and Kawano Masanori Memorial Public InterestIncorporated Foundation for Promotion of Pediatrics (Y. Sakai).

CONFLICT OF INTEREST

None.

AUTHOR CONTRIBUTIONS

D. Kang, S. Kanba, Y. Nakabeppu, Y. Sakai and S. Ohga designed research; S. Akamine, S. Okuzono, H. Yamamoto, D. Setoyama, N. Sagata, M. Ohgidani, Y. Matsushita, H. Ono, H. Kato, K. Masuda and T. Ishitani performed research; TA Kato, Y. Ishizaki, M. Sanefuji, H. Saitsu H and N. Matsumoto analyzed data; S. Akamine, Y. Sakai, and S. Ohga wrote the paper.

ORCID

Yasunari Sakai https://orcid.org/0000-0002-5747-8692

REFERENCES

1. McTague A, Howell KB, Cross JH, Kurian MA, Scheffer IE. The genetic landscape of the epileptic encephalopathies of infancy and childhood. *Lancet Neurol*. 2016;15:304-316.
2. Takata A, Nakashima M, Saitsu H, et al. Comprehensive analysis of coding variants highlights genetic complexity in developmental and epileptic encephalopathy. *Nat Commun*. 2019;10:2506.
3. Scheffer IE, Berkovic S, Capovilla G, et al. ILAE classification of the epilepsies: Position paper of the ILAE commission for classification and terminology. *Epilepsia*. 2017;58:512-521.
4. Ohtahara S, Ohtsuka Y, Yamatogi Y, Oka E. The early-infantile epileptic encephalopathy with suppression-burst: developmental aspects. *Brain Dev*. 1987;9:371-376.
5. Lombroso CT. Early myoclonic encephalopathy, early infantile epileptic encephalopathy, and benign and severe infantile myoclonic epilepsies: a critical review and personal contributions. *J Clin Neurophysiol*. 1990;7:380-408.
6. Coppola G, Plouin P, Chiron C, Robain O, Dulac O. Migrating partial seizures in infancy: a malignant disorder with developmental arrest. *Epilepsia*. 1995;36:1017-1024.
7. Hamdan FF, Myers CT, Cossette P, et al. High rate of recurrent de novo mutations in developmental and epileptic encephalopathies. *Am J Hum Genet*. 2017;101:664-685.
8. Epi KC, Phenome E, Genome P, et al. De novo mutations in epileptic encephalopathies. *Nature*. 2013;501:217-221.
9. Nakamura K, Kodera H, Akita T, et al. De Novo mutations in GNAO1, encoding a Galphao subunit of heterotrimeric G proteins, cause epileptic encephalopathy. *Am J Hum Genet*. 2013;93:496-505.
10. Saitsu H, Fukai R, Ben-Zeev B, et al. Phenotypic spectrum of GNAO1 variants: epileptic encephalopathy to involuntary movements with severe developmental delay. *Eur J Hum Genet*. 2016;24:129-134.
11. Danti FR, Galosi S, Romani M, et al. GNAO1 encephalopathy: broadening the phenotype and evaluating treatment and outcome. *Neurol Genet*. 2017;3:e143.
12. Schorling DC, Dietel T, Evers C, et al. Expanding phenotype of de novo mutations in GNAO1: four new cases and review of literature. *Neuropediatrics*. 2017;48:371-377.
13. Feng H, Khalil S, Neubig RR, Sidiropoulos C. A mechanistic review on GNAO1-associated movement disorder. *Neurobiol Dis*. 2018;116:131-141.
14. Gerald B, Ramsey K, Belnap N, et al. Neonatal epileptic encephalopathy caused by de novo GNAO1 mutation misdiagnosed as atypical Rett syndrome: cautions in interpretation of genomic test results. *Semin Pediatr Neurol*. 2018;26:28-32.
15. Feng H, Sjogren B, Karaj B, Shaw V, Gezer A, Neubig RR. Movement disorder in GNAO1 encephalopathy associated with gain-of-function mutations. *Neurology*. 2017;89:762-770.
16. Lambright DG, Noel JP, Hamm HE, Sigler PB. Structural determinants for activation of the alpha-subunit of a heterotrimeric G protein. *Nature*. 1994;369:621-628.
17. Kozasa T, Hepler JR, Smrcka AV, et al. Purification and characterization of recombinant G16 alpha from Sf9 cells: activation of purified phospholipase C isozymes by G-protein alpha subunits. *Proc Natl Acad Sci U S A*. 1993;90:9176-9180.
18. Valenzuela D, Han X, Mende U, et al. G alpha(o) is necessary for muscarinic regulation of Ca2+ channels in mouse heart. *Proc Natl Acad Sci U S A*. 1997;94:1727-1732.
19. Feng H, Larrivee CL, Demireva EY, Xie H, Leipprandt JR, Neubig RR. Mouse models of GNAO1-associated movement disorder: allele- and sex-specific differences in phenotypes. *PLoS ONE*. 2019;14:e0211066.
20. Jiang M, Gold MS, Boulay G, et al. Multiple neurological abnormalities in mice deficient in the G protein Go. *Proc Natl Acad Sci U S A*. 1998;95:3269-3274.
21. Saitsu H, Tohyama J, Kumada T, et al. Dominant-negative mutations in alpha-II spectrin cause West syndrome with severe cerebral hypomyelination, spastic quadriplegia, and developmental delay. *Am J Hum Genet*. 2010;86:881-891.
22. Syrbe S, Harms FL, Parrini E, et al. Delineating SPTAN1 associated phenotypes: from isolated epilepsy to encephalopathy with progressive brain atrophy. *Brain*. 2017;140:2322-2336.
23. Wang Y, Ji T, Nelson AD, et al. Critical roles of alphaII spectrin in brain development and epileptic encephalopathy. *J Clin Invest*. 2018;128:760-773.
24. Ohkubo K, Sakai Y, Inoue H, et al. Moyamoya disease susceptibility gene RNF213 links inflammatory and angiogenic signals in endothelial cells. *Sci Rep*. 2015;5:13191.

25. Matsushita Y, Sakai Y, Shimmura M, et al. Hyperactive mTOR signals in the proopiomelanocortin-expressing hippocampal neurons cause age-dependent epilepsy and premature death in mice. *Sci Rep*. 2016;6:22991.
26. Sakai Y, Shaw CA, Dawson BC, et al. Protein interactome reveals converging molecular pathways among autism disorders. *Sci Transl Med*. 2011;3:86ra49.
27. Shevchenko A, Tomas H, Havlis J, Olsen JV, Mann M. In-gel digestion for mass spectrometric characterization of proteins and proteomes. *Nat Protoc*. 2006;1:2856-2860.
28. The UniProt C. UniProt: the universal protein knowledgebase. *Nucleic Acids Res*. 2017;45:D158-D169.
29. Sagata N, Kato TA, Kano SI, et al. Dysregulated gene expressions of MEX3D, FOS and BCL2 in human induced-neuronal (iN) cells from NF1 patients: a pilot study. *Sci Rep*. 2017;7:13905.
30. Nguyen Nguyen HT, Kato H, Sato H, et al. Positive effect of exogenous brain-derived neurotrophic factor on impaired neurite development and mitochondrial function in dopaminergic neurons derived from dental pulp stem cells from children with attention deficit hyperactivity disorder. *Biochem Biophys Res Commun*. 2019;513:1048-1054.
31. Naito Y, Hino K, Bono H, Ui-Tei K. CRISPRdirect: software for designing CRISPR/Cas guide RNA with reduced off-target sites. *Bioinformatics*. 2015;31:1120-1123.
32. Ran FA, Hsu PD, Wright J, Agarwala V, Scott DA, Zhang F. Genome engineering using the CRISPR-Cas9 system. *Nat Protoc*. 2013;8:2281-2308.
33. Eiraku M, Watanabe K, Matsuo-Takasaki M, et al. Self-organized formation of polarized cortical tissues from ESCs and its active manipulation by extrinsic signals. *Cell Stem Cell*. 2008;3:519-532.
34. Robu ME, Larson JD, Nasevicius A, et al. p53 activation by knockdown technologies. *PLoS Genet*. 2007;3:e78.
35. Vasanwala FH, Kusam S, Toney LM, Dent AL. Repression of AP-1 function: a mechanism for the regulation of Blimp-1 expression and B lymphocyte differentiation by the B cell lymphoma-6 protooncogene. *J Immunol*. 2002;169:1922-1929.
36. Akamine S, Sagata N, Sakai Y, et al. Early-onset epileptic encephalopathy and severe developmental delay in an association with de novo double mutations in NF1 and MAGEL2. *Epilepsia Open*. 2018;3:81-85.
37. Baldwin PR, Curtis KN, Patriquin MA, et al. Identifying diagnostically-relevant resting state brain functional connectivity in the ventral posterior complex via genetic data mining in autism spectrum disorder. *Autism Res*. 2016;9:553-562.
38. Kato H, Thi Mai Pham T, Yamaza H, et al. Mitochondria regulate the differentiation of stem cells from human exfoliated deciduous teeth. *Cell Struct Funct*. 2017;42:105-116.
39. McCartney CE, MacLeod JA, Greer PA, Davies PL. An easy-to-use FRET protein substrate to detect calpain cleavage in vitro and in vivo. *Biochim Biophys Acta Mol Cell Res*. 2018;1865:221-230.
40. Veeranna, Kaji T, Boland B, et al. Calpain mediates calcium-induced activation of the erk1,2 MAPK pathway and cytoskeletal phosphorylation in neurons: relevance to Alzheimer's disease. *Am J Pathol*. 2004;165:795-805.
41. Tyagarajan SK, Ghosh H, Yevenes GE, et al. Extracellular signal-regulated kinase and glycogen synthase kinase 3beta regulate gephyrin postsynaptic aggregation and GABAergic synaptic function in a calpain-dependent mechanism. *J Biol Chem*. 2013;288:9634-9647.
42. Yap EL, Greenberg ME. Activity-regulated transcription: bridging the gap between neural activity and behavior. *Neuron*. 2018;100:330-348.
43. Sakaguchi H, Ozaki Y, Ashida T, et al. Self-organized synchronous calcium transients in a cultured human neural network derived from cerebral organoids. *Stem Cell Reports*. 2019;13:458-473.
44. Lancaster MA, Renner M, Martin CA, et al. Cerebral organoids model human brain development and microcephaly. *Nature*. 2013;501:373-379.
45. Amin ND, Pasca SP. Building models of brain disorders with three-dimensional organoids. *Neuron*. 2018;100:389-405.
46. Tanaka Y, Cakir B, Xiang Y, Sullivan GJ, Park IH. Synthetic analyses of single-cell transcriptomes from multiple brain organoids and fetal brain. *Cell Rep*. 2020;30:1682-1689.e3.
47. Watanabe M, Buth JE, Vishlaghi N, et al. Self-organized cerebral organoids with human-specific features predict effective drugs to combat Zika virus infection. *Cell Rep*. 2017;21:517-532.
48. Galiano MR, Jha S, Ho TS, et al. A distal axonal cytoskeleton forms an intra-axonal boundary that controls axon initial segment assembly. *Cell*. 2012;149:1125-1139.
49. Huang CY, Zhang C, Ho TS, et al. alphaII spectrin forms a periodic cytoskeleton at the axon initial segment and is required for nervous system function. *J Neurosci*. 2017;37:11311-11322.
50. Xu K, Zhong G, Zhuang X. Actin, spectrin, and associated proteins form a periodic cytoskeletal structure in axons. *Science*. 2013;339:452-456.
51. Hama H, Kurokawa H, Kawano H, et al. Scale: a chemical approach for fluorescence imaging and reconstruction of transparent mouse brain. *Nat Neurosci*. 2011;14:1481-1488.
52. Ming G, Song H, Berninger B, Inagaki N, Tessier-Lavigne M, Poo M. Phospholipase C-gamma and phosphoinositide 3-kinase mediate cytoplasmic signaling in nerve growth cone guidance. *Neuron*. 1999;23:139-148.
53. Luchtenborg AM, Solis GP, Egger-Adam D, et al. Heterotrimeric Go protein links Wnt-Frizzled signaling with ankyrins to regulate the neuronal microtubule cytoskeleton. *Development*. 2014;141:3399-3409.
54. Jiang M, Bajpayee NS. Molecular mechanisms of go signaling. *Neurosignals*. 2009;17:23-41.
55. Katanaev VL, Ponzielli R, Semeriva M, Tomlinson A. Trimeric G protein-dependent frizzled signaling in Drosophila. *Cell*. 2005;120:111-122.
56. Kurian MA, Meyer E, Vassallo G, et al. Phospholipase C beta 1 deficiency is associated with early-onset epileptic encephalopathy. *Brain*. 2010;133:2964-2970.
57. Hillenbrand M, Schori C, Schoppe J, Pluckthun A. Comprehensive analysis of heterotrimeric G-protein complex diversity and their interactions with GPCRs in solution. *Proc Natl Acad Sci U S A*. 2015;112:E1181-E1190.
58. Lau BYC, Othman A. Evaluation of sodium deoxycholate as solubilization buffer for oil palm proteomics analysis. *PLoS ONE*. 2019;14:e0221052.
59. Raucher D, Sheetz MP. Phospholipase C activation by anesthetics decreases membrane-cytoskeleton adhesion. *J Cell Sci*. 2001;114:3759-3766.
60. Zhou R, Han B, Xia C, Zhuang X. Membrane-associated periodic skeleton is a signaling platform for RTK transactivation in neurons. *Science*. 2019;365:929-934.

61. Leterrier C, Dargent B. No Pasaran! Role of the axon initial segment in the regulation of protein transport and the maintenance of axonal identity. *Semin Cell Dev Biol*. 2014;27:44-51.
62. Rasband MN. The axon initial segment and the maintenance of neuronal polarity. *Nat Rev Neurosci*. 2010;11:552-562.
63. Leterrier C. The axon initial segment, 50 years later: a nexus for neuronal organization and function. *Curr Top Membr*. 2016;77:185-233.
64. Rasmussen HB, Frokjaer-Jensen C, Jensen CS, et al. Requirement of subunit co-assembly and ankyrin-G for M-channel localization at the axon initial segment. *J Cell Sci*. 2007;120:953-963.
65. Wimmer VC, Reid CA, So EY, Berkovic SF, Petrou S. Axon initial segment dysfunction in epilepsy. *J Physiol*. 2010;588:1829-1840.
66. Yoshimura T, Kawano Y, Arimura N, Kawabata S, Kikuchi A, Kaibuchi K. GSK-3beta regulates phosphorylation of CRMP-2 and neuronal polarity. *Cell*. 2005;120:137-149.
67. Jenkins SM, Bennett V. Ankyrin-G coordinates assembly of the spectrin-based membrane skeleton, voltage-gated sodium channels, and L1 CAMs at Purkinje neuron initial segments. *J Cell Biol*. 2001;155:739-746.
68. Ackermann A, Brieger A. The role of nonerythroid spectrin alphaII in cancer. *J Oncol*. 2019;2019:7079604.
69. Pearson TS, Helbig I. Epileptic encephalopathy, movement disorder, and the yin and yang of GNAO1 function. *Neurology*. 2017;89:754-755.

SUPPORTING INFORMATION

Additional Supporting Information may be found online in the Supporting Information section.

How to cite this article: Akamine S, Okuzono S, Yamamoto H, et al. *GNAO1* organizes the cytoskeletal remodeling and firing of developing neurons. *The FASEB Journal*. 2020;34:16601–16621. https://doi.org/10.1096/fj.202001113R

GNAO1 organizes the cytoskeletal remodeling and firing of developing neurons

Satoshi Akamine, Sayaka Okuzono, Hiroyuki Yamamoto, Daiki Setoyama, Noriaki Sagata, Masahiro Ohgidani, Takahiro A. Kato, Tohru Ishitani, Hiroki Kato, Keiji Masuda, Yuki Matsushita, Hiroaki Ono, Yoshito Ishizaki, Masafumi Sanefuji, Hirotomo Saitsu, Naomichi Matsumoto, Dongchong Kang, Shigenobu Kanba, Yusaku Nakabeppu, Yasunari Sakai, and Shouichi Ohga

This file contains 15 figures (Fig S1 to S15)

Tables S1 and S2 are available at: https://1drv.ms/b/s!Ahn0JZjkrgCQgTJRMD98-CQEO_KG?e=N0C43O

Table S1. Oligonucleotide primers and antibodies used in this study

Table S2. Summary of co-immunoprecipitation and mass spectrometry

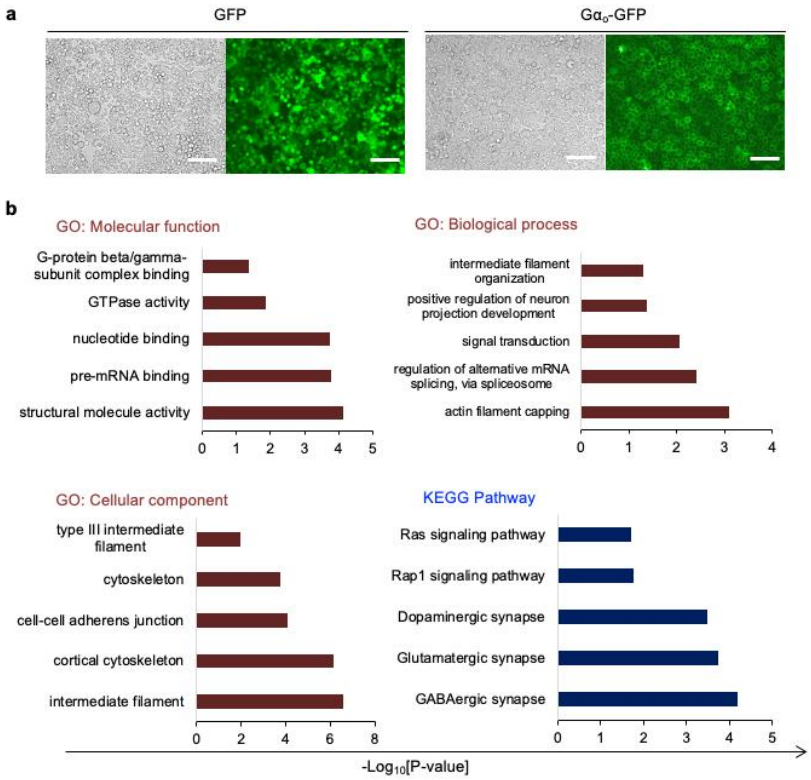

Figure S1. Proteomic analysis of Gαo-binding proteins

a. Establishment of Neuro2a stable cell lines, expressing GFP or GFP-$G\alpha_O$. Light field (left) and green fluorescence (right) of the cells are shown. Scale bar, 100 μm.

b. Gene Ontology (GO) and Kyoto Encyclopedia of Genes and Genomes (KEGG) pathway analyses. Database search was carried out after the conversion of detected peptides to human homologs. Bar plots represent the $-\log_{10}$ [P value] data of top 5 lists in "Molecular function", "Biological process", "Cellular component" of GO domains and KEGG database.

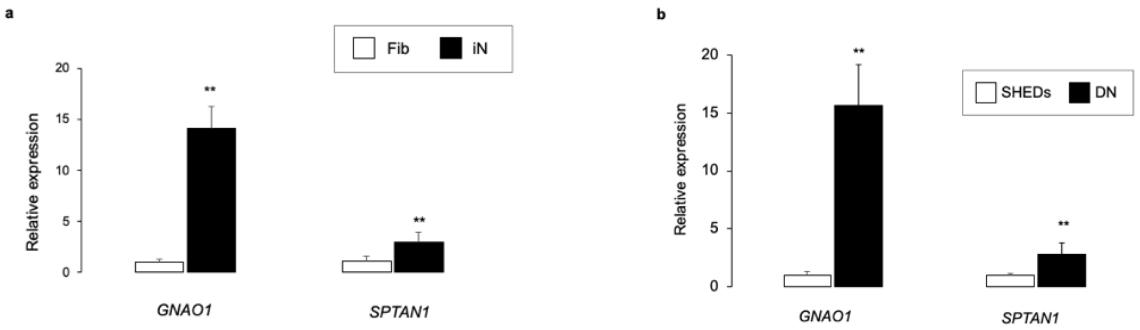

Figure S2. Co-expression of *GNAO1* and *SPTAN1* in human cells

a. *GNAO1* and *SPTAN1* mRNAs in human fibroblasts (Fib, n = 9) and induced neurons (iN, n = 9). Data are shown as the mean ± SD values. *p < 0.05, **p < 0.01 (Student's *t*-test).

b. *GNAO1* mRNA in human mesenchymal stem cells and dopaminergic neurons from deciduous teeth (SHEDs, n = 9) and *in vitro* differentiated neurons (DNs, n = 9).

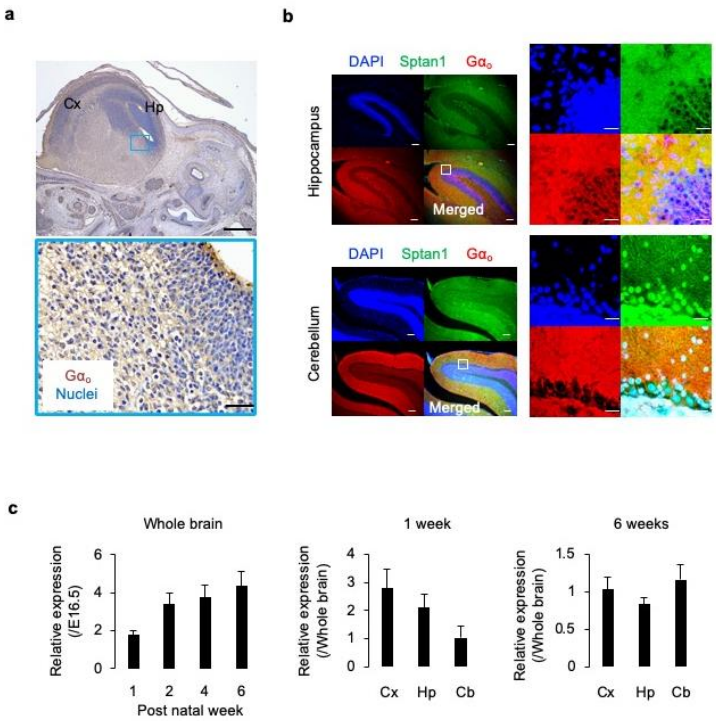

Figure S3. Spatial co-expression of Gα$_O$ and Sptan1 proteins *in vivo*

a. Immunohistochemistry of the murine brain at E16. Gα$_O$-positive cells (brown) are present in the whole brain. The lower panel shows a higher magnification of the selected region (blue square). Gα$_O$ signals are detected at the cell membrane. Scale bar, 500 µm (4x) and 100 µm (20x).

b. Immunofluorescence images of the dentate gyrus (upper) and cerebellum (lower) of wild- type mice at two weeks old. Note the co-localized signals of Gα$_O$ (green) and Sptan1 (red) in the molecular layers (ML) of the two regions. Scale bar, 100 µm (4x) and 20 µm (20x).

c. High-expression profile of *Gnao1* in the postnatal brain of wild-type mice. The bar plots show the relative mRNA level of *Gnao1*/*Actb* in the whole brain at each age (1 – 6 weeks) to that at E16.5 (left) and indicated brain regions (middle and right). Data are shown as mean ± SD values (n = 6). Cx, cerebral cortex; Hp, hippocampus; and Cb, cerebellum.

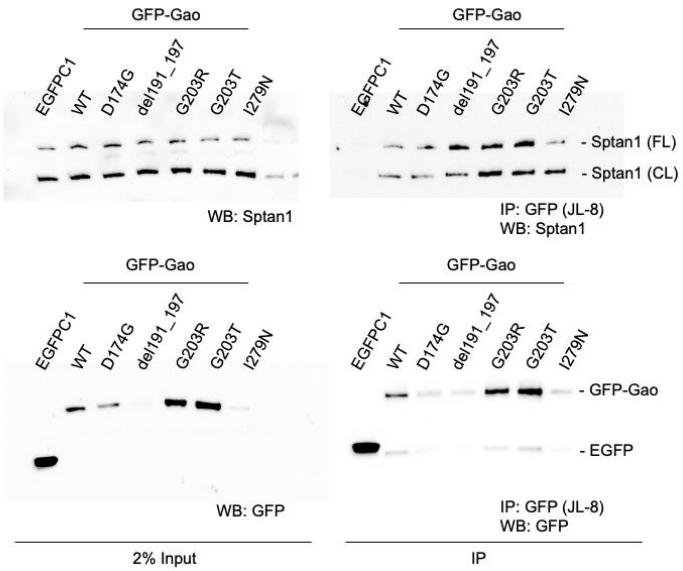

Figure S4. Interaction of the wild-type and mutant Gao proteins with Sptan1. Representative western blots for the extracted proteins (2% input, left) and those after co-immunoprecipitation with anti-GFP (IP, right). Empty (EGFPC1) or Gao-expressing plasmids were transfected to Neuro2a cells. Note that the GFP-tagged wild-type (WT) and mutant Gao proteins were expressed at variable levels in Neuro2a cells (lower panels). Interaction of WT and mutant Gao with Sptan1 appeared to vary with the expression levels of Gao proteins (right upper panel).

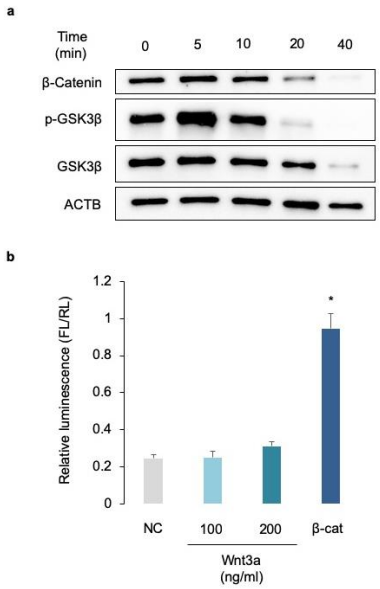

Figure S5. Wnt signaling in the wild-type and mutant Gαo-expressing cells

a. Expression of ß-catenin in Neuro2a cells after stimulation with ionomycin (1 μM). Note that GSK3ß was phosphorylated immediately after the stimulation, whereas the expression of ß-catenin was not increased during the time course (0 – 40 min).

b. TOP-Flash reporter assay in Neuro2a cells after stimulation with the synthetic mouse Wnt3a ligand. Note that Wnt3a at either 100 or 200 ng/ml did not activate the TOP-Flash reporter. Constitutive-active beta-catenin (ß-cat) was used for the positive control. Renilla luciferase reporter (pRL-TK, Clontech) was used as internal control. Data are shown as mean ± SD values (n = 4). *$p < 0.05$ (Student's *t*-test).

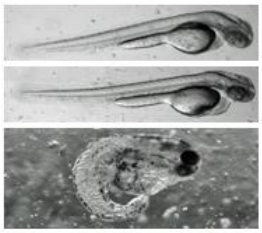

MO	Malformation (%)	Low Activity (%)
p53	21/114 (18)	11/103 (11)
p53 + Vehicle		
p53 + *gnao1*	68/92 (74)*	28/60 (47)*

Figure S6. The neurodevelopmental effects of morpholino antisense oligonucleotides on the fertilized embryo of zebrafish. Morpholino (MO) to the Danio rerio homolog of GNAO1 (gnao1) or to p53 (negative control) was microinjected into the embryos at the single-cell stage. Malformation in general appearance and body movements was analyzed on agarose gel at 72 hr post-fertilization. *p < 0.05, Chi-square test.

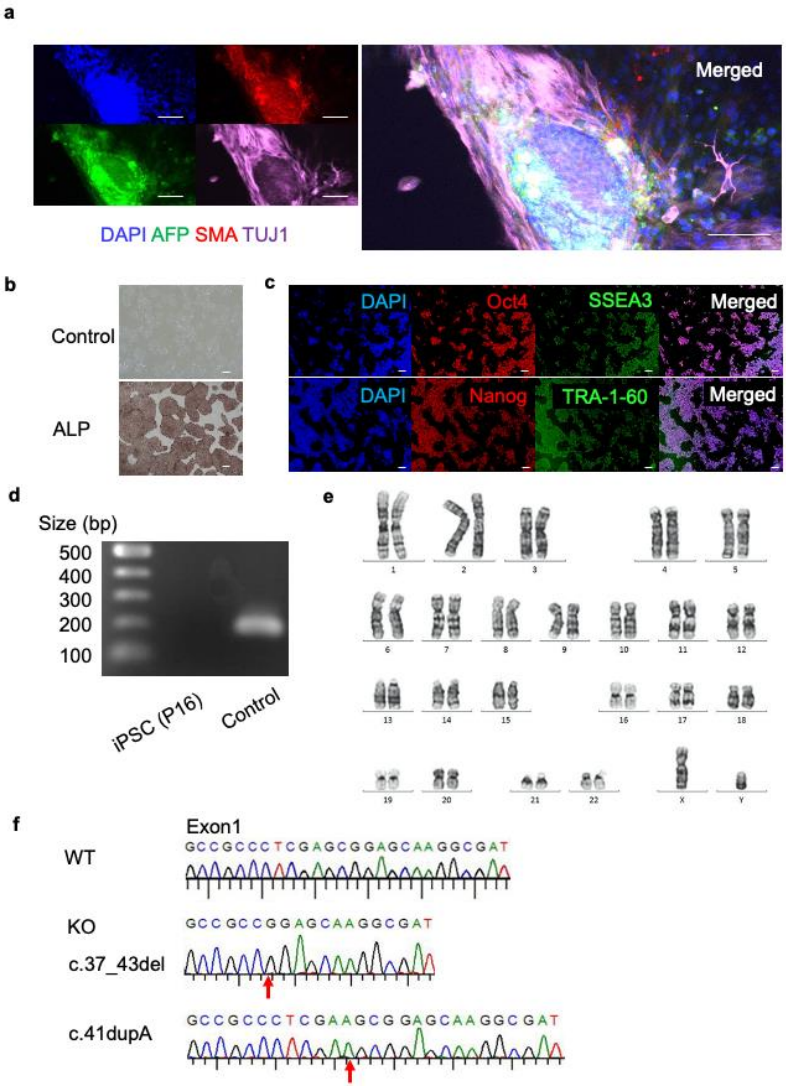

Figure S7. Induced pluripotent stem cells from a healthy volunteer

a. Differentiation of induced pluripotent stem (iPS) cells into three germ layers. Endoderm (AFP, green), mesoderm (SMA, red) and ectoderm markers (TUJ1, magenta) were used in the immunofluorescence study. Scale bar, 100 µM. For panels A and C, DAPI was used for nuclear staining.

b. Expression of alkaline phosphatase (ALP) in iPS cells. Transparent image (upper) and immunohistochemistry

data with anti-ALP antibody (lower) are shown. Scale bar, 20 μM.

c. Immunofluorescence images of iPS cells with Oct4, SSEA3, Nanog and TRA-1-60 signals. Scale bar, 20 μM.

d. Absence of Sendai virus vector in the iPS cells at passage 16. An aliquot of vector DNA (Control) and the test sample (iPS P16) were amplified with the same PCR system. Note that the target amplicon (200 bp) appears in Control, but not in iPS P16.

e. The G-band test for iPS cells shows the normal male karyotype (46,XY). Disruption of the *GNAO1* gene by CRISPR/Cas9 system.

f. Chromatograms show the results of Sanger sequencing for iPS cells with the wild-type allele (top), those with a 7-base deletion (c.37_43del, middle) and a one-base insertion (c.42dupA, bottom) in the exon 1 of *GNAO1*.

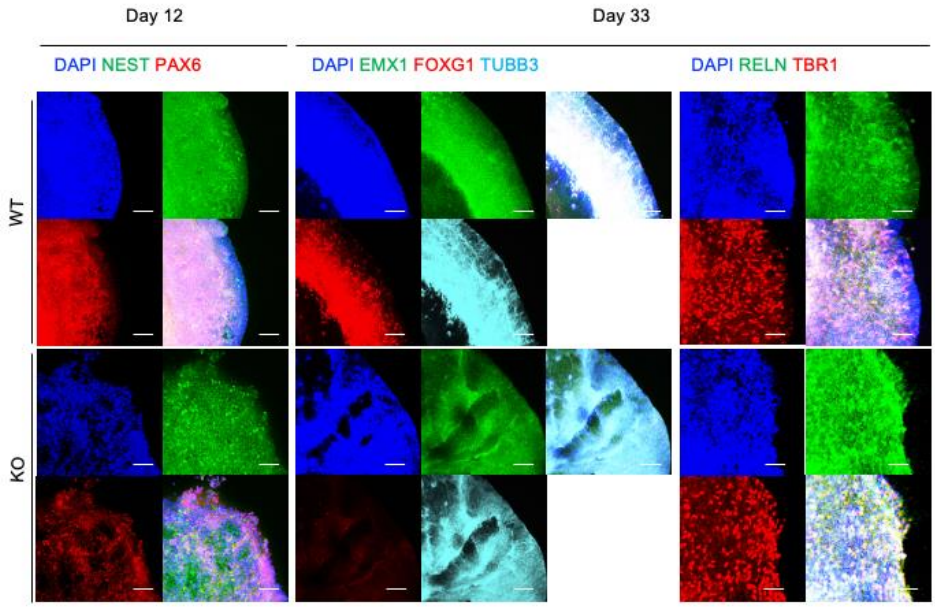

Figure S8. Immunofluorescence images of WT and KO spheroids at 12 and 33 days. WT and KO spheroids expressed comparable levels of neuronal lineage markers (Nestin, PAX6, FOXG1, EMX1, and TUBB3) and mature neuronal markers (TBR1 and Reelin) at the indicated days of differentiation.

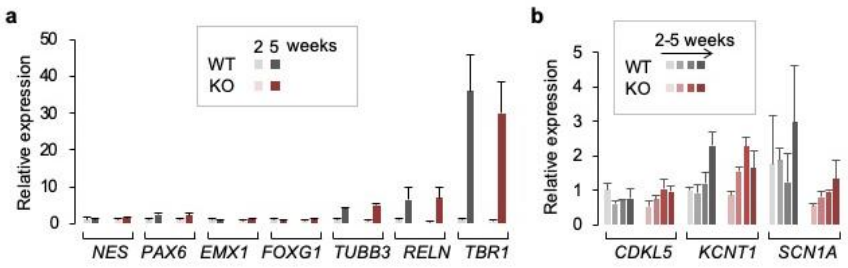

Figure S9. Expressions of neuronal markers and DEE-associated genes in spheroids.

a. Quantitative (q) PCR for neuronal markers (mRNAs) at 2 and 5 weeks of differentiation.

b. qPCR for DEE-associated genes (*CDKL5*, *KCNT1*, and *SCN1A*) from 2 to 5 weeks of differentiation. No significant difference in the gene expression was observed between WT and KO spheroids (*a* and *b*). Data are shown as mean ± SD values (n = 4).

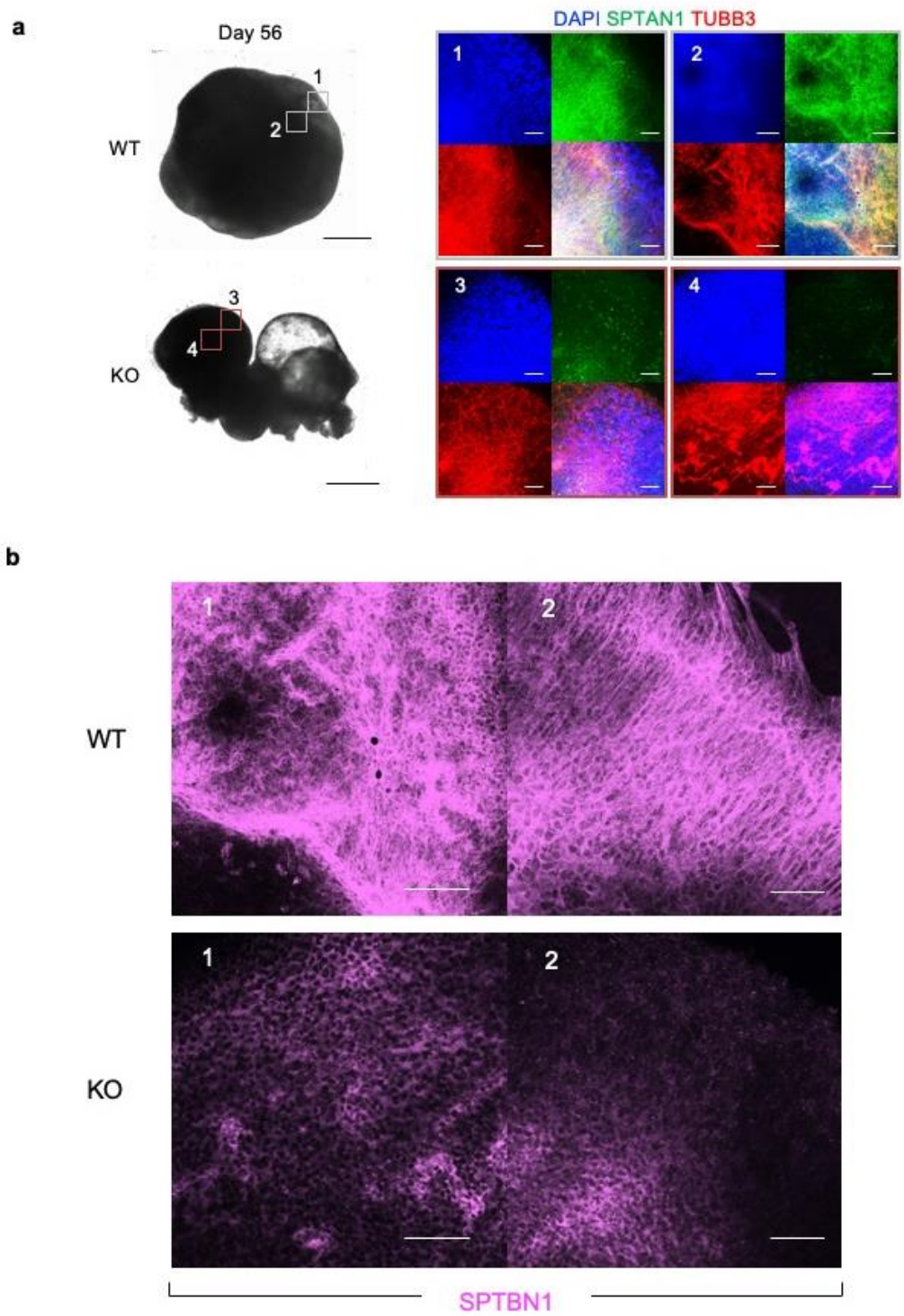

Figure S10. Dysmorphic features of *GNAO1*-KO spheroids at the advanced stage of differentiation.

a. Overview of WT and *GNAO1*-KO spheroids at 56 days of differentiation. The numbered regions of interest (WT: 1, 2 and KO: 3 and 4) correspond to the immunofluorescence images on the right. Scale bar, 50 µM. WT and KO neuro-spheroids at day 56 were counter-immunolabeling with SPTAN1, TUBB3 and DAPI. Scale bar, 50 µM.

b. Spheroids at day 56 were counter-immunolabeling with SPTBN1 (magenta) in addition to SPTAN1, TUBB3 and DAPI (panel a). The numbering of each panel corresponds to that in panel a (WT: 1, 2 and KO: 3 and 4). Scale bar, 50 µM.

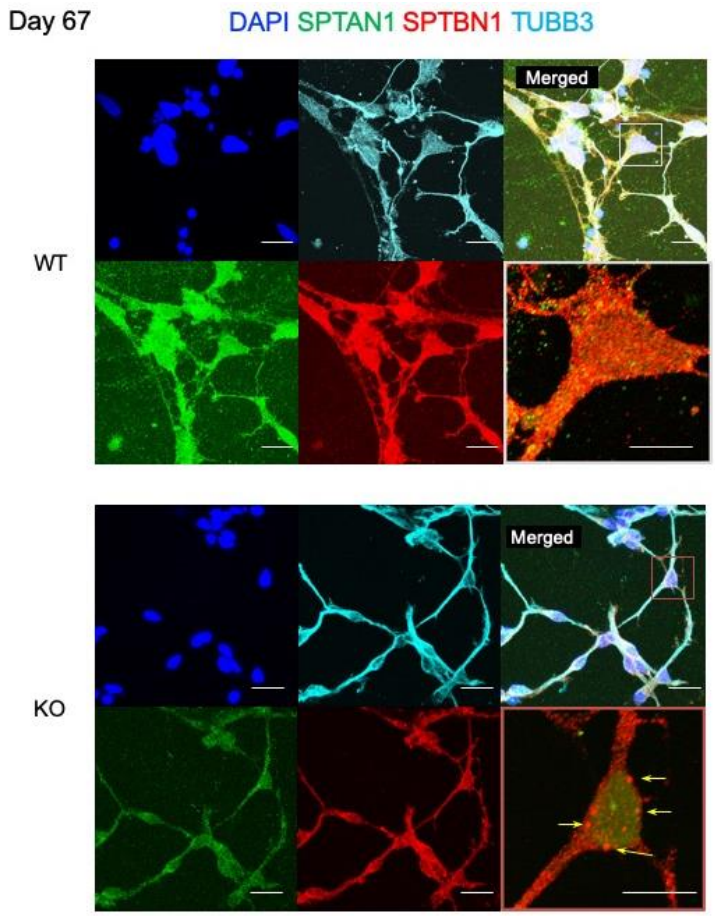

Figure S11. A microscopic analysis of WT and *GNAO1*-KO neurons at a higher magnification. Gray and red-brown squares indicate the regions of interest for WT and *GNAO1*-KO neurons, respectively. Scale bar, 20 µM (gray square) and 10 µM (red-brown square).

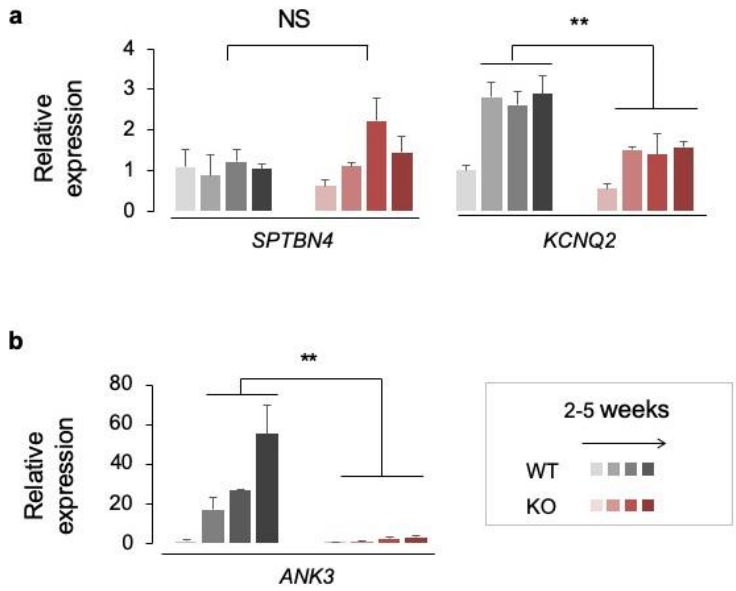

Figure S12. Expression profiles of the axon initial segment-associated genes in neurospheroids. Quantitative PCR data for the genes, *SPTBN4*, *KCNQ2* (a), and *ANK3* (b) during 2 – 5 weeks of differentiation. Data are shown as mean ± SD values (n = 4). **p < 0.01 (Student's *t*-test).

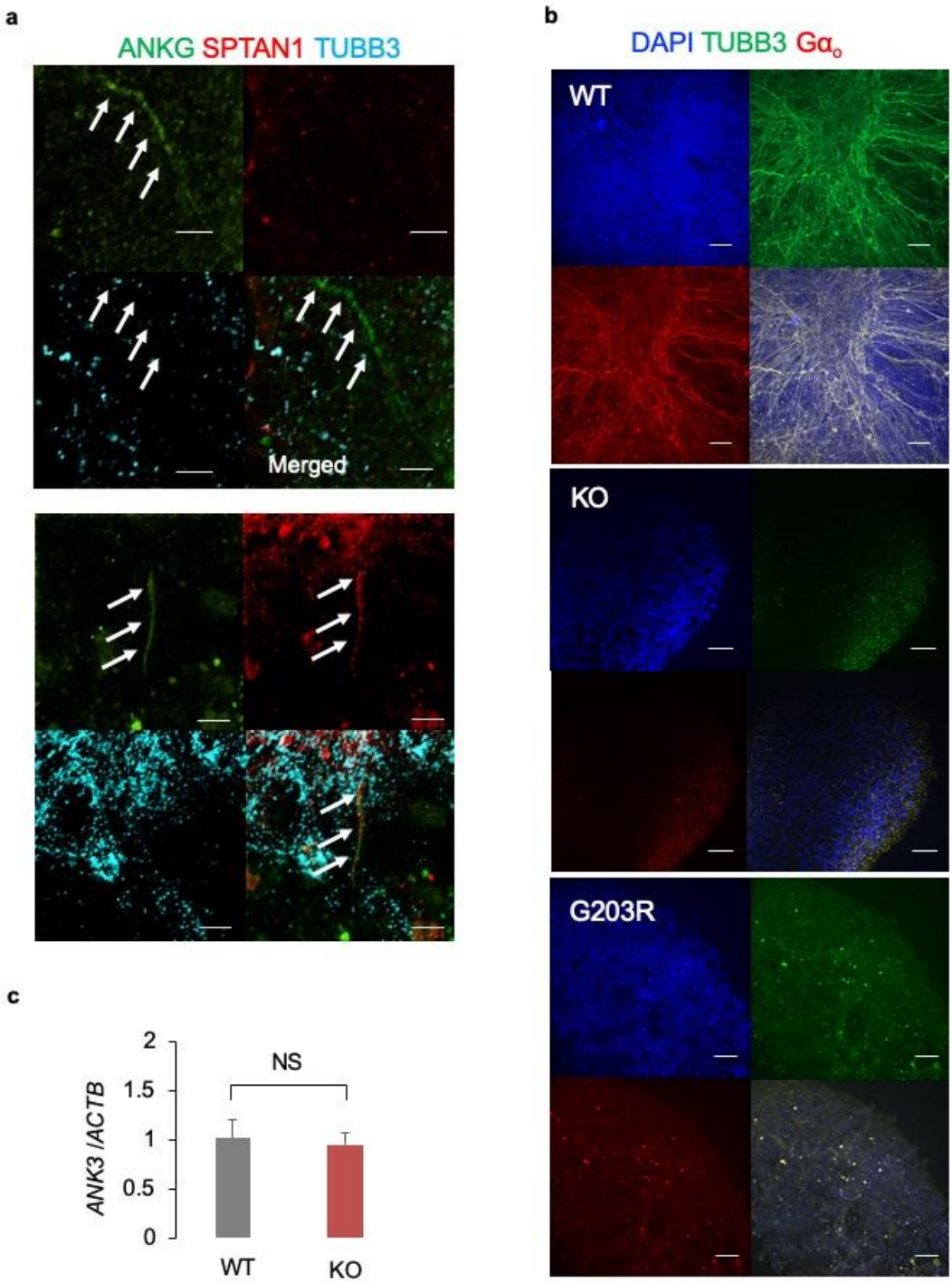

Figure S13. The axon initial segment-like structure in cortical organoids at 100 days of differentiation.

a. Two representative images of rod-shaped AnkG signals (green) in mature organoids at 15 weeks (100 days) of differentiation. SPTAN1 (red) and TUBB3 (cyan) signals are shown in triple-color images. Scale bar, 5μM.

b. Stacked images of WT, KO, and Pt (G203R) organoids obtained via stimulated emission depletion (STED) microscopy. $G\alpha_O$-TUBB3-positive neurites show extension in the WT organoids but not in the KO or Pt (G203R) organoids. Scale bar, 50 μm.

c. Quantitative PCR for *ANK3* in WT and KO organoids at 31 weeks (220 days) of differentiation. NS, not significant. Data are shown as mean ± SD values (n = 4).

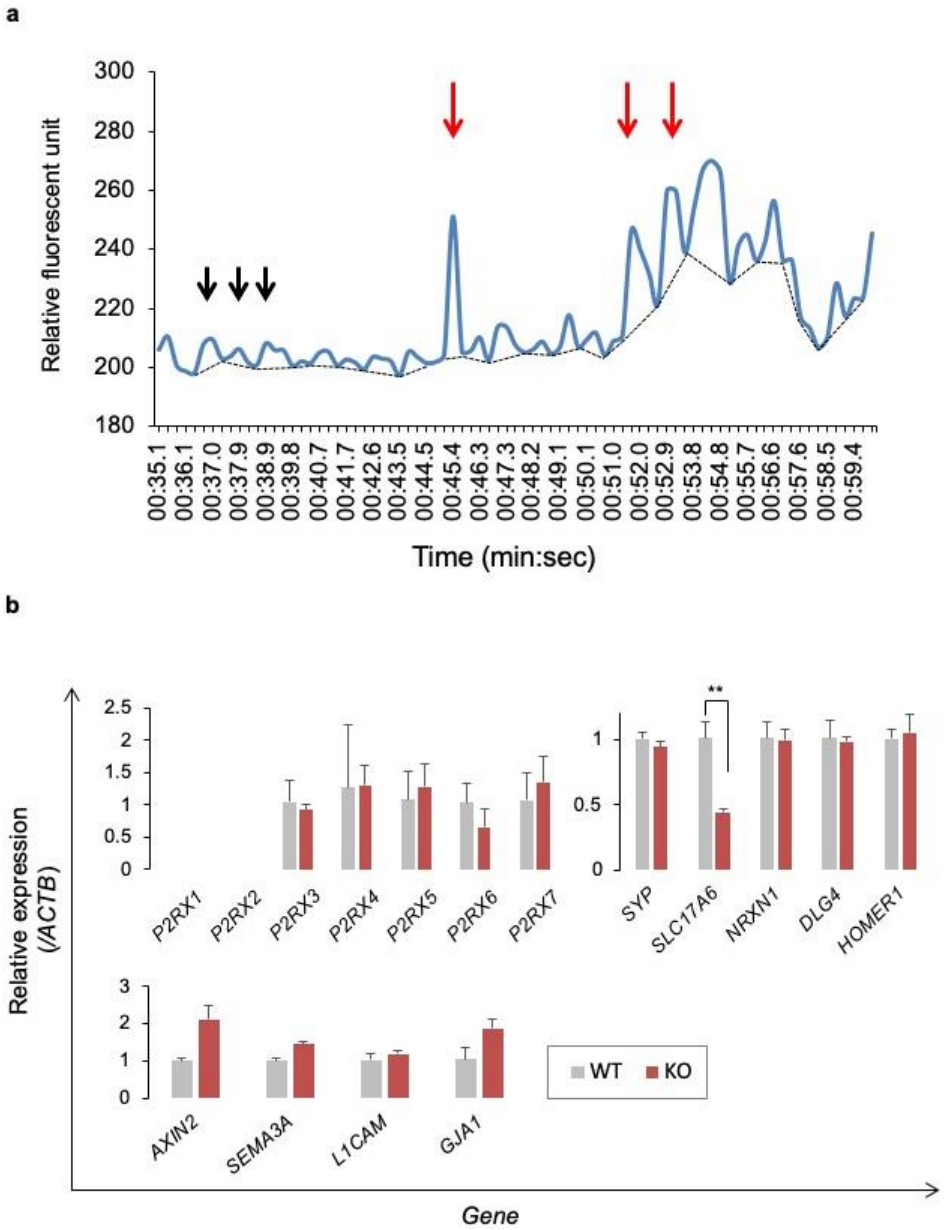

Figure S14. Defective firing of KO neurons

a. Oscillation and firing activity of neurons. A representative trace for the Fluo4 signals (ROI1 in WT) indicates the oscillating activity (black arrows) and spontaneous firing of neurons (red arrows). Dashed lines denote the base line for the measurement of firing amplitude. The frequency of neuronal activity with ≥ 30 RFU was counted for "firing rate" in the quantitative analysis.

b. Expression profiles of purinergic receptor-coding genes (*P2RX1 – 7*, upper left panel); pre- (*SYP*, *SLC17A6*, *NRXN1*) and post-synaptic molecules (*DLG4* and *HOMER*, upper right); and Wnt/ß-catenin-associated genes (*AXIN2*, *SEMA3A*, *L1CAM*, *GJA1*, lower panel) in WT and KO organoids. Organoids at more than 40 weeks of differentiation were used in this assay. Note that KO organoids expressed normally purinergic receptor-coding genes, significantly lower level of *SLC17A6* (*VGLUT2*), whereas higher levels of Wnt/ß-catenin-associated genes. Relative expression of indicated genes to *ACTB* were analyzed with quantitative PCR. Data are shown as man ± SD (n = 4). *p < 0.05 (Student's *t*-test).

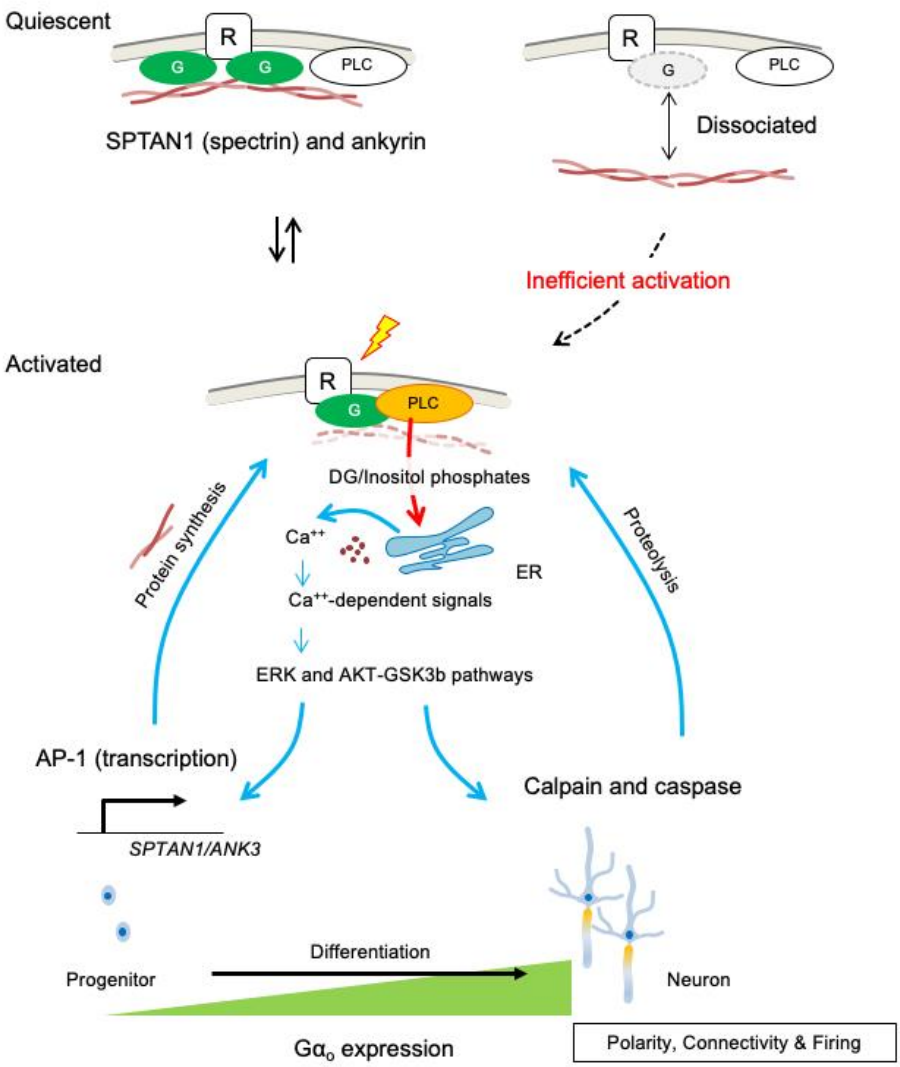

Figure S15. A proposed model for the cooperative function of Gao with SPTAN1 in cytoskeletal remodeling and neuronal differentiation. This model shows the versatile roles of Gao during differentiation of neurons from progenitor cells. Upon receiving the extracellular ligand stimulation, membrane-bound receptor (R), Gao (green ovals) and SPTAN1 (orange and blue rods) complex efficiently activate PLC beta (PLC) and calcium releases from endoplasmic reticulum (ER). Calcium (Ca^{++})-dependent signals and downstream pathways (ERK and AKT-GSK3 beta) consequently induce AP1-dependent transcription of *SPTAN1* and other cytoskeleton-encoding genes (*ANK3*). In parallel, activated signals enhance calpain and caspase-mediated proteolysis of cytoskeletal proteins. The cytoskeletal remodeling assists the neurite outgrowth, acquisition of dendro-axonal polarity, neural connectivity, and firing in differentiating neurons. These activation process might be disturbed in patients with *GNAO1*-associated encephalopathy. In the right upper panel, "G" (white-gray oval) represents the functional loss of Gao.